2011

Effect of Step Change in Growth Speed During Directional Solidification on Array Morphology of Al-7 Wt Si Alloy

Swapna Pakiru
Cleveland State University

EFFECT OF STEP CHANGE IN GROWTH SPEED DURING DIRECTIONAL SOLIDIFICATION ON ARRAY MORPHOLOGY OF Al -7 WT% Si ALLOY

SWAPNA PAKIRU

Bachelor of Chemical Engineering

Jawaharlal Nehru Technological University

April 2007

Submitted in partial fulfillment of requirements for the degree

MASTER OF SCIENCE IN CHEMICAL ENGINEERING

at the

CLEVELAND STATE UNIVERISTY

CLEVELAND, OHIO

December 2011

This Thesis has been approved

for the department of Chemical and Biomedical Engineering

and the College of Graduate Studies by

_____

Dr. Surendra N Tewari
Thesis committee Chair Person

_____
Date

Chemical and Biomedical Engineering

_____

Dr. Dhananjai B Shah

_____
Date

Chemical and Biomedical Engineering

_____

Dr.Orhan Talu

_____
Date

Chemical and Biomedical Engineering

ACKNOWLEDGEMENTS

I take this opportunity to express my sincere Gratitude and thanks to my Graduate advisor, Dr. Surendra Nath Tewari for his valuable guidance, encouragement and support during the course of my study at Cleveland State University. He will always be a source of inspiration throughout my life.

I would also thank my committee members: Dr. D. B. Shah, Dr. Orhan Talu for reading of the manuscript and helpful suggestions. I would like to convey my sincere thanks to my colleagues, Dr. Siva Kumar Ramasamy, Mr. Ravi Shankar Rajamure, Mr. Ufuk Sarikaya, Ms. Arianna A Romano and Mr. Mohammad mofidfar for their help and friendship.

I also greatly appreciate the support from Ms. Becky Laird and Ms. Darlene Montgomery for their constant encouragement, help and caring during the course of my studies.

Finally, I would like to extend my heart full thanks to my Parents, cousins and friends, their support and blessings had made this work possible.

Support for this research was provided by the Microgravity Materials Research Program at NASA – Marshall Space Flight Center (Huntsville, AL).

This Thesis is dedicated to

My Parents

&

Late: P. Ranga Reddy (Grandfather)

Late: P. Anthamma (Grandmother)

EFFECT OF STEP CHANGE IN GROWTH SPEED ON ARRAY MORPHOLOGY DURING DIRECTIONAL SOLIDIFICATION OF Al – 7 WT% Si ALLOY

SWAPNA PAKIRU

ABSTRACT

Dendritic single crystals of Al-7wt%Si alloy have been directionally solidified at a thermal gradient of 40 K cm^{-1} over growth speeds, ranging from 5 to 85 to 31µm s^{-1}, using aluminum single crystal seed aligned along [100] crystallographic orientation. Mushy zone morphology parameters, such as, primary dendrite nearest neighbor spacing, primary dendrite trunk diameter, side (secondary dendrite) branch length and side branch orientation, have been characterized in to investigate the transients introduced by step increase and step decrease in growth speed.

An increase in the growth speed shows a decrease in both nearest neighbor spacing and trunk diameter. A comparison between the two parameters suggests that the trunk-diameter may be a better metric to quantify differences due to small change in processing parameters, such as, growth in low-gravity in the absence of convection. The trend of decreasing trunk diameter with increasing growth speed is similar to the primary dendrite tip radii trend (predicted by theoretical models). Statistical analysis of the transverse microstructures after the step decrease in growth speed (from 85 to 31µm s^{-1}) showed that primary dendrites which survive the transient are the ones with larger neighbor spacing. However, the predictive ability of nearest-neighbor distance (NNS-1), mean of four

nearest neighbor distances (NNS-4) or the mean of six nearest neighbor distances (NNS-6) in terms of which dendrites are likely to dissolve-off appears to be similar. Average side-branch length of the surviving primary dendrites increases and those of the disappearing primary dendrites decreases after the growth speed decrease. Primary dendrites whose side-arms are not orthogonal are more likely to dissolve-off than those which are aligned closer to [100]. Porosity formation during directional solidification can lead to spurious grain formation which will seriously degrade the high temperature creep properties of directionally solidified components.

TABLE OF CONTENTS

LIST OF FIGURES

Figure **Page**

LIST OF TABLES

Table **Page**

CHAPTER I

INTRODUCTION

1.1. Solidification of alloys

Solidification is a phenomenon by which a molten liquid is transformed into a solid component. When a molten alloy is brought in contact with a cold surface three distinct regions develop, as shown in Figure 1[1]: the liquid, the liquid plus solid (called mushy zone), and the solid. It is the mushy zone where all the micro-structural characteristics, such as, the shape, size, and distributions of dendrites, precipitates, and pores, and the concentration inhomogeneities (micro and macro segregation) are determined. The solidification behavior in the mushy zone also determines defects, such as, feeding related shrinkages and hot tearing. Some of the important processes which involve solidification are casting, welding, soldering/brazing, rapid solidification processing, directional solidification etc.

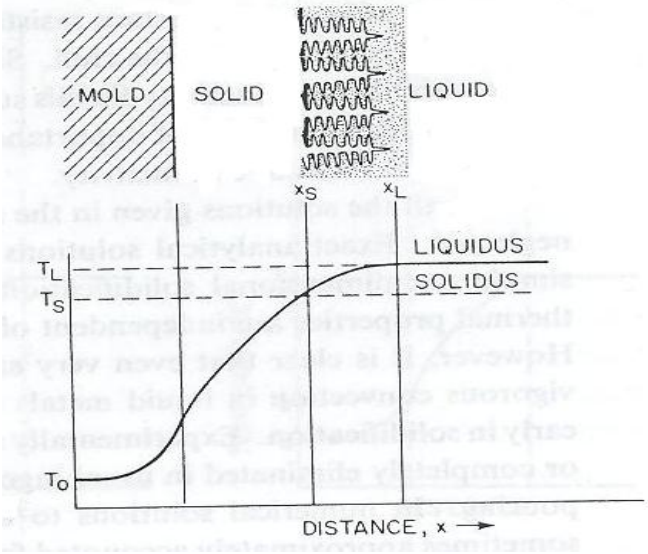

Figure 1. Temperature profile of an alloy against a flat mold wall.

The growth morphology during solidification also depends upon the way in which the latent heat of fusion is carried away from the liquid-solid interface, as shown in Figure 2[2]. Growth into an under-cooled melt where the latent heat of fusion is dissipated through the cooler liquid ahead of the interface results in the formation of equiaxed dendritic grains (Figure 2a). Whereas growth into a positive thermal gradient in which heat is extracted from the colder solidifying solid end results in columnar dendritic crystals form (Figure 2b).

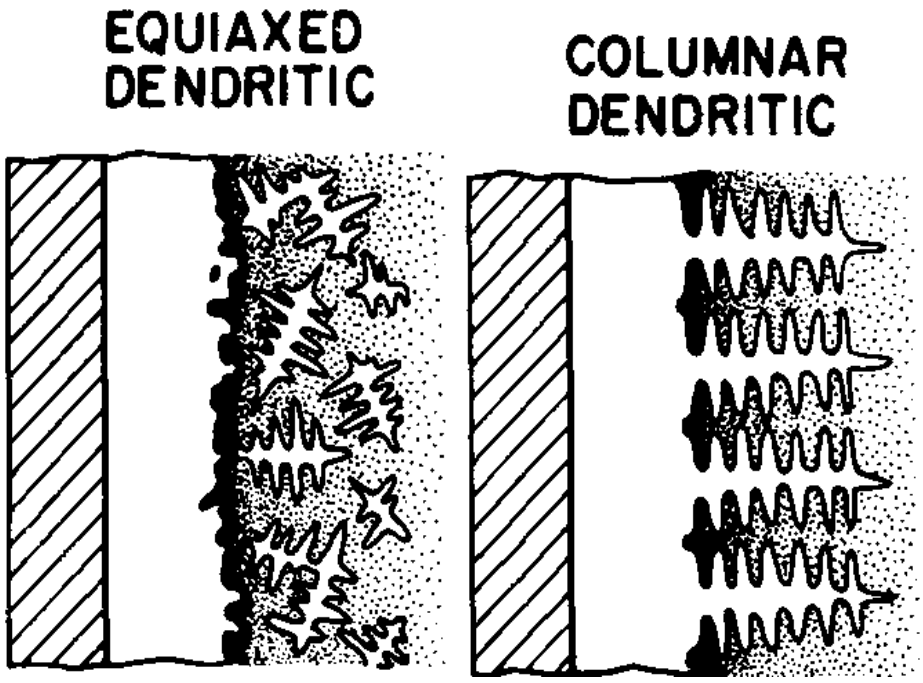

2 (a): Equiaxed grains (2b): Columnar grains.

Figure 2. Equiaxed and columnar dendritic morphology during solidification: equiaxed dendrites during growth in an undercooled melt and columnar dendrites during growth in a positive thermal gradient.

The grain boundaries resulting from equiaxed morphology are major source of weakness, especially in components used for high temperature applications, such as gas turbine engine blade and vane. The cavities forming at the grain boundaries, transverse to the loading axis, due to grain boundary sliding at high temperatures decrease creep life. The creep life of such components is increased significantly by generating columnar grains which are aligned parallel to the loading axis by directional solidification. The columnar grain morphology is obtained by controlled directional solidification of alloys.

1.2. Directional Solidification

As shown schematically in Figure 3 below, the hot and the cold zones of a directional solidification (DS) furnace are separated by an adiabatic zone which enables heat extraction only along the longitudinal direction allowing the solidification to proceed in a directional manner. This allows independent control of the two important solidification parameters, the thermal gradient at the liquid-solid interface (G) and the liquid-solid interface speed (solidification speed, R).

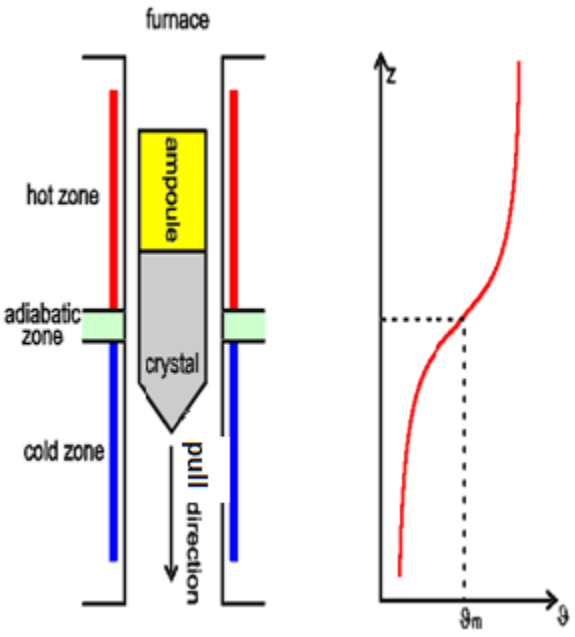

Figure 3. Typical directional solidification furnace.

For a given alloy composition (solute content C_o for a binary alloy, for example) the liquid-solid interface can be planar (high G/R), cellular (intermediate G/R), or columnar dendritic (low G/R). A typical columnar dendritic morphology during directional solidification of a binary alloy is shown in Figure 4.

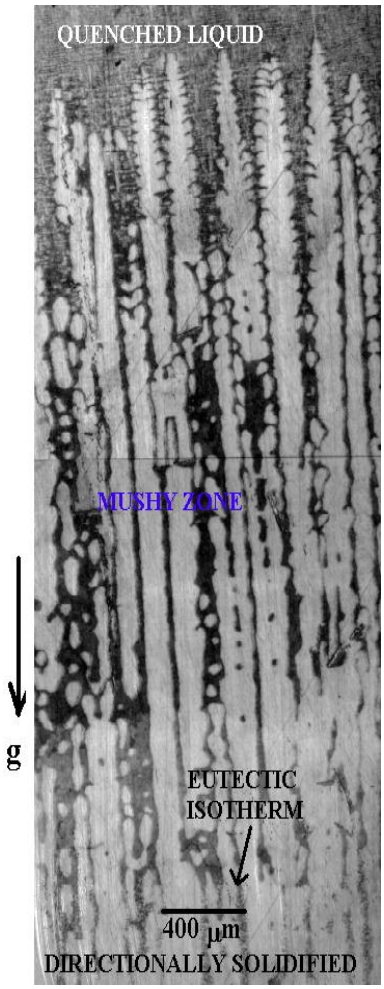

Density Inversion => Interdendritic

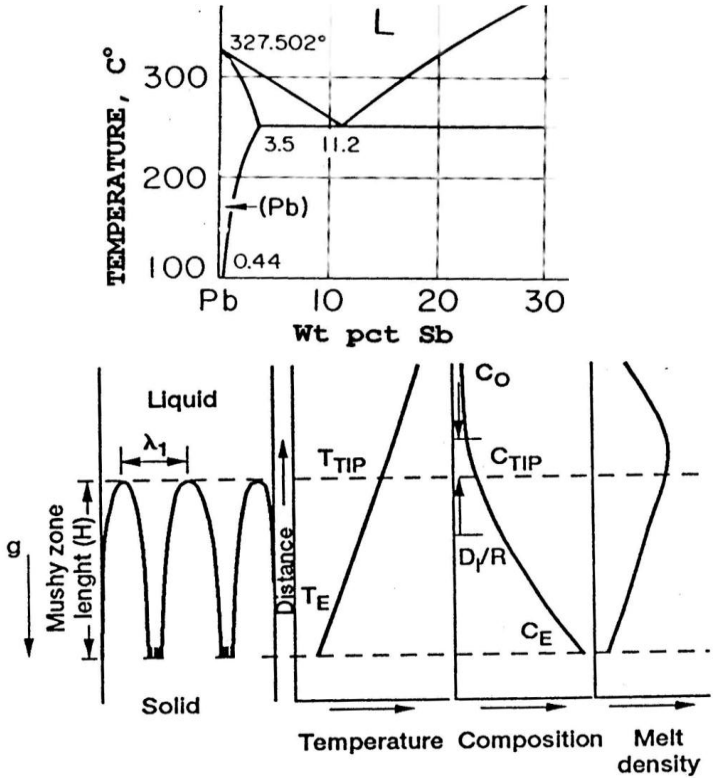

- Reduction in Primary Dendrite Spacing

(a) (b)

Figure 4. Mushy zone morphology during directional solidification of a binary Pb-8 wt% Sb alloy [3].

As shown in Figure 4(a) the quenched liquid is at the top, the columnar dendritic array in the middle and the completely solidified portion at the bottom. The mushy zone extends from the liquidus temperature of the alloy at the top to the eutectic temperature at the bottom. Dendritic array microstructure is similar to an X-mass tree where the longitudinal

tree trunk is called as the primary dendrite and the protrusions (branches) coming off the main trunk are the secondary dendrite. The branches coming off the secondary are called tertiary dendrites. The corresponding inter-dendritic spacing's are called primary dendrite spacing; secondary dendrite spacing and tertiary dendrite spacing respectively; they are function of G, R and C_o.

As shown schematically in Figure 4(b), the positive thermal gradient, hotter liquid on top of the cooler melt, is stabilizing against natural convection in the mushy zone. However, under a constant thermal gradient, the difference between the solute solubility in the liquid and the solid phases results in rejection of solute ahead of the solidifying liquid-solid interface creating a solutal gradient in the melt. This concentration gradient can lead to the density inversion in the liquid (for alloys where the solute is less dense than the solvent, such as Pb-Sn, or Pb-Sb), which can cause convection in the presence of gravity. The convective flow makes the solidification process non-homogenous. It is shown to result in many morphological defects such as "channel segregate formation", "primary dendrite clustering", short and long length (compared with primary dendrite spacing) compositional inhomogeneities, called micro and macro-segregation, and formation of misaligned or equiaxed grains in an otherwise DS component. A good review of macro-segregation has been presented by Grugel and Brush [4].

Such microstructural defects are especially detrimental for gas turbine engine blade application, where significant mechanical property advantage is achieved by having the entire blade made-up of single crystal, oriented along [100] crystallographic direction [5, 6]

1.3. Purpose of the study

The main purpose of this study is to carry out a quantitative evaluation of the various mushy-zone morphology parameters due to step-change in growth speed during directional solidification of Al-7 wt% Si at one constant thermal gradient, such as, primary dendrite trunk diameter, primary dendrite nearest neighbor spacing and magnitude and orientation of the side branches (secondary dendrites), and identify which morphology parameter is likely to most readily respond to growth speed changes. The second purpose of this study was to examine the role of convection or other defects on the formation of "spurious" (misoriented) grains during directional solidification.

The Al-7% Si alloy was selected for this study because the density of aluminum and silicon are similar [7]**,** this is expected to minimize any density inversion driven convection in the mushy zone. Its phase diagram, presented below in Figure 5 [8], and thermo physical properties [9], presented in the Table 1, are well characterized.

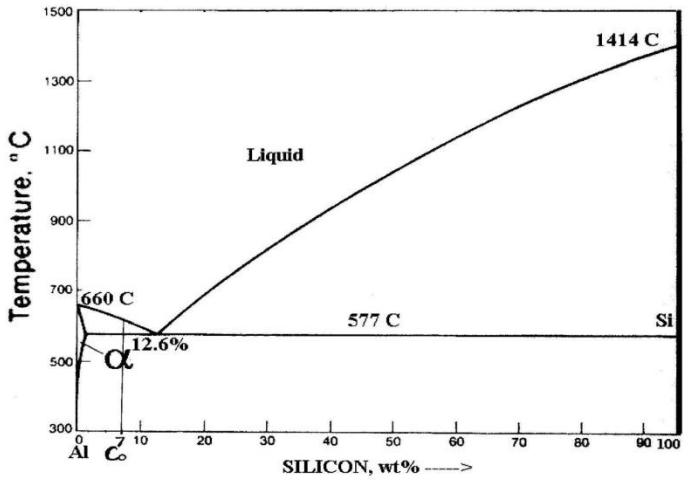

Figure 5. Al-Si phase diagram.

Table 1: Thermo physical Properties of Aluminum - 7 wt % Silicon Alloy

1) Liquidus Temperature (T_l, ˚C)	614
2) Liquidus Slope (m (α), K/wt %)	6.62
3) Solute partition coefficient (k (α))	0.13
4) Eutectic Temperature (T_e, ˚C (K))	577(850)
5) Eutectic Composition (C_e, wt %)	12.6
6) Heat of Fusion (Δh_f, J/m^3)	-9.5*10^8
7) Entropy of Fusion (ΔS_f, J/m^3 k)	-1.02*10^6
8) Gibbs-Thomson Coefficient (Γ, μmK)	0.12
9) Solutal Capillary length (m)	2.9*10^{-9}

CHAPTER II

EXPERIMENTAL PROCEDURE

2.1. Raw materials and preparation of the alloy

Al-7wt%Si alloy, 20 to 30 cm long and 9- mm diameter as cast feed-stock used for directional solidification was prepared from 99.99% pure Aluminum (Al) and 99.99% pure Silicon. The as cast feed-stock bars were very kindly supplied by Dr. Men G. Chu, Technical Fellow-Solidification Technology, ALCOA Technical Center, Pittsburgh PA. Chemical Analysis of the alloy is given below.

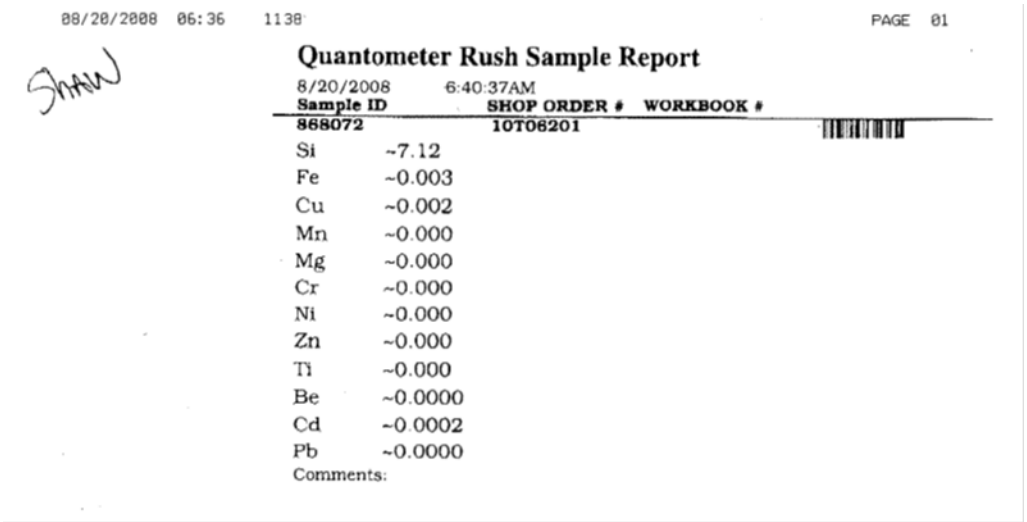

08/20/2008 06:36 1138 PAGE 01

SHAW

Quantometer Rush Sample Report

8/20/2008 6:40:37AM

Sample ID	SHOP ORDER #	WORKBOOK #
868072	10T06201	

Si	~7.12
Fe	~0.003
Cu	~0.002
Mn	~0.000
Mg	~0.000
Cr	~0.000
Ni	~0.000
Zn	~0.000
Ti	~0.000
Be	~0.0000
Cd	~0.0002
Pb	~0.0000

Comments:

2.2. Directional Solidification Apparatus

Bridgeman directional solidification apparatus, employed for the Directional Solidification (DS), is shown in Figure 6. The graphite susceptor, hanging inside a double walled, water-cooled, cylindrical quartz enclosure is heated by using an RF power by the help of an induction coil. The susceptor kept inside a zirconia cylinder acts as the heated furnace in this set-up. A dynamic vacuum of $2X10^{-4}$ torr is maintained within the quartz enclosure. A refractory disk of about 1.2 cm thickness kept at the bottom of the heating zone works as the adiabatic zone. Sample cooling at the bottom is via radiation cooling. The alloy feed-stock kept in a graphite crucible is inserted into the furnace, melted and then withdrawn from the furnace at the predetermined growth speed to carry out the directional solidification. The RF power setting is adjusted and controlled to the thermal gradient during directional solidification.

Figure 6. RF heated Directional solidification furnace.

2.3. Temperature Profile during the directional solidification

Figure 7 shows a typical graphite crucible used for directional solidification. The three chromel-alumel thermocouples (T_{C1}, T_{C2} and T_{C3}), placed outside the graphite crucible, with their tips embedded into the graphite wall are used to record the thermal profile along the sample length. A [100] oriented single crystal aluminum seed was first used to create [100] oriented Al-7% Si alloy dendritic single crystal feed stock. A portion from this seed was placed in the crucible bottom below the as-cast feed stock bar. The furnace was heated, the graphite crucible was raised into the furnace to a predetermined height which ensured that only a portion of the [100] seed kept at the bottom melted and fused

with the rest of the melt on the top. The sample was usually held stationary for about half-hour to achieve a steady-state thermal profile before its withdrawal from the furnace to carry out the directional solidification.

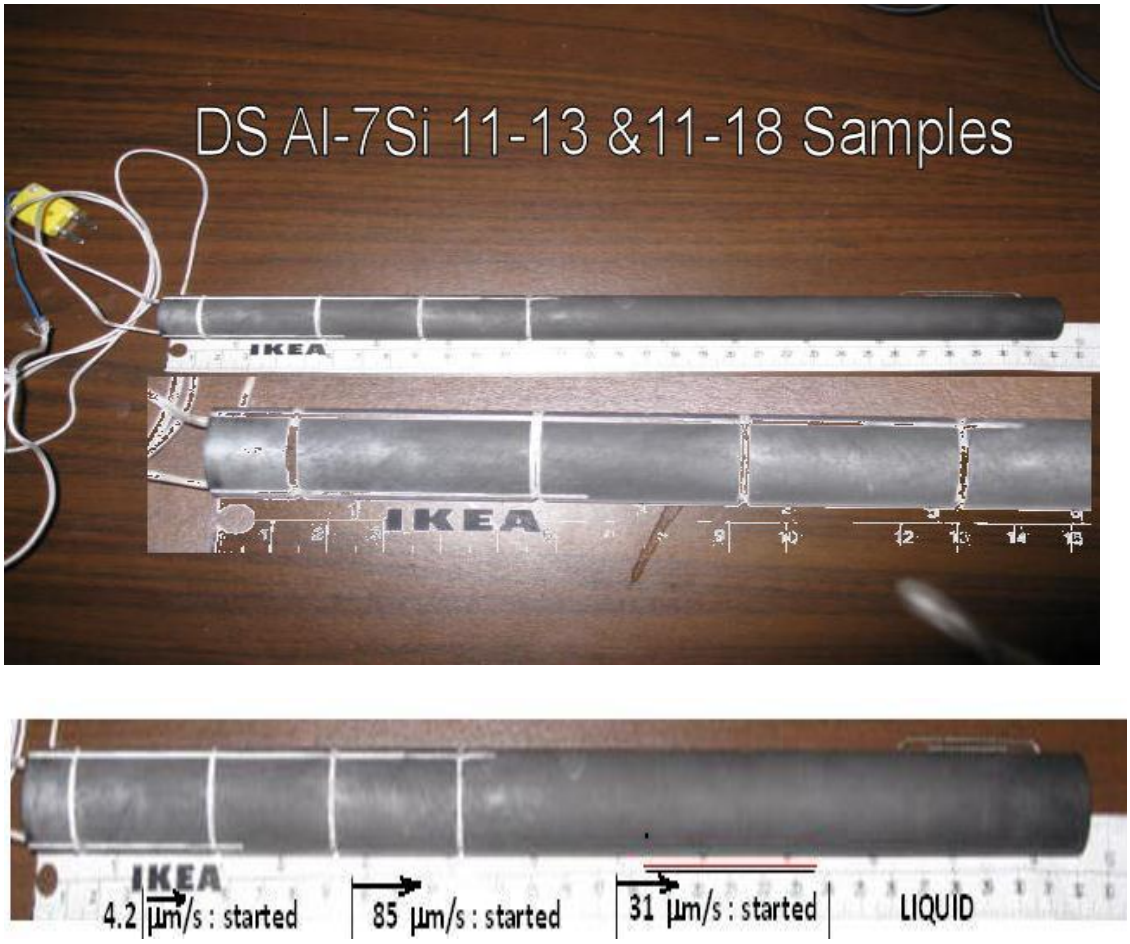

Figure 7. Graphite crucible embedded with the three thermocouples along the crucible length when different growth speeds were used. After remelting a portion of the seed, directional solidification was carried out at 4.2, 85, and 31 µm s^{-1}.

Figure 8 shows the temperature profiles recorded by the three thermocouples with the hot-zone temperature at 685^{o}C during the directional solidification of Al-7 wt % Si alloy at various growth speeds for directionally solidified 11-13 sample, which was grown at 4 µm s^{-1}, then, introduced a step-increase in the growth speed to 85 µm $s^{-1}$and finally step

decrease in the growth speed to 31 μm s^{-1}. The thermal gradient (G_l) in the melt ahead of the dendrite array tips at the liquidus temperature recorded by the three thermocouples T_{C1}, T_{C2} and T_{C3} are 42, 41 and 38 K cm^{-1} respectively. The average of three thermal values, 41 K cm^{-1}, is used as the thermal gradient value for this experiment.

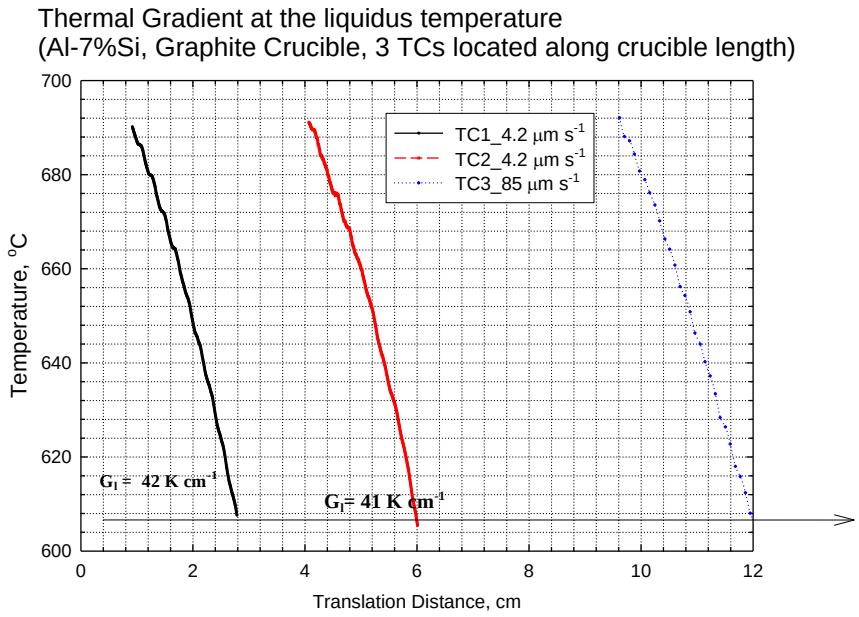

Figure 8. Thermal profiles recorded by three thermocouples during directional solidification.

2.4. Sample Preparation and Metallography

Directionally solidified alloy sample was taken out from the graphite crucible and two grooves were inscribed along the sample length to mark the reference for transverse (cross-section) microstructures. These references allow one to stack transverse images so that any particular region of a transverse section can be examined in terms of any morphology change, such as, rotation of primary dendrites or formation of spurious grains. Transverse slices of about 3.8 mm were cut along the sample length, making sure that hot end for each sample slice was identified for subsequent sample mounting and

polishing. The samples mounted using a 1.25 inch diameter phenolic resin mould, were ground and polished on a Buehler automatic grinder and polisher using the following protocol.

Grit-Grade	**Force/Sample**	**Time(min)**	**RPM**
400(Grinding)	3 lbs	1	120
600(Grinding)	3 lbs	1	120
800(Polishing)	3 lbs	2	120
1200(Polishing)	3 lbs	2	120
3-µm diamond suspension	4 lbs	5	120
1-µm diamond suspension	4 lbs	5	120
0.05 µm colloidal silica	4 lbs	10	120

The polished samples were etched by an etchant made-up 190 ml of distilled water (H_2O), 2ml of Hydrochloric acid (HCl), 5 ml of Nitric acid (HNO_3) and 2 ml of Hydro fluoric acid (HF). A thick cotton swab was taken and soaked in the etchant. Then the cotton swab was gently rubbed on the polished surface of the sample for about five to ten seconds and placed under cold stream water. Finally the sample was dried and used for microstructure examination.

The etched samples were examined by an optical micro-scope using HL Image++ 98 software at a magnification of 50-X. Considering the entire cross-section of 9 mm diameter sample nearly 70 to 150 optical pictures were taken to create a montage of entire sample cross-section by the help of Jasc Paint Shop Pro software .

2.5. Image Analysis

2.5.1. Nearest neighbor spacing using dendrites centers of primary dendrites

The montages of transverse sections of the sample were saved in BMP image format. The BMP images were opened in Image analysis software, Sigma Scan Pro 4.0 to measure X and Y coordinates (dendrite center). From the "measure" menu list, "trace measurement options" was selected which displayed a window with available measurements to be added into the dialog box, "X" and "Y "were selected and added into the dialog box. Then from the "tools" menu, "pixel pointer" of size one was selected to measure the dendrite center(X, Y), i.e., the cross-section center of primary dendrites in the transverse section. When the center of dendrite was marked with the pixel pointer the corresponding (X, Y) values were generated in Sigma scan Pro worksheet and the data were compiled with the aid of C-Program [10] to calculate the nearest neighbor spacing (NNS) between the dendrites.

Figure 9 shows a typical sample cross-section and the corresponding locations of the dendrite-centers. Please note that in this picture the dendrite center markings (one pixel in size) have been made much larger than one pixel for the ease of illustration. Figure 10 shows a typical primary-dendrite center distribution across an entire 9-mm diameter sample cross-section. Again, in this figure, the centers have been enlarged (larger than one pixel) for the ease of visualization.

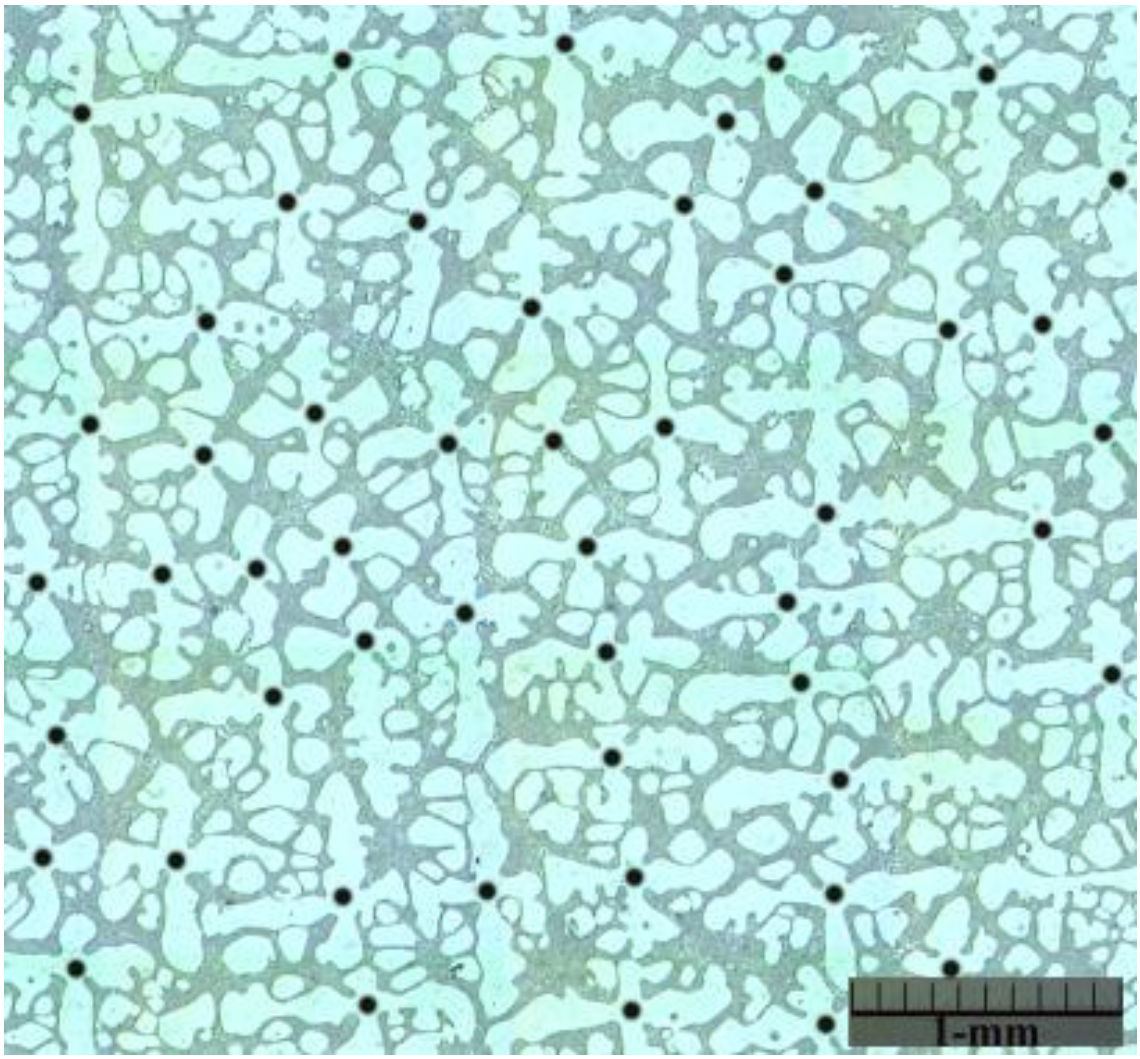

Figure 9. Measurement of dendrite centers (x, y) points typically shown on Transverse Microstructure of an Al – 7 wt% Si Alloy which is obtained at Growth Velocity (R) =72 μm s^{-1} and Thermal Gradient = 40 K cm^{-1}.

.

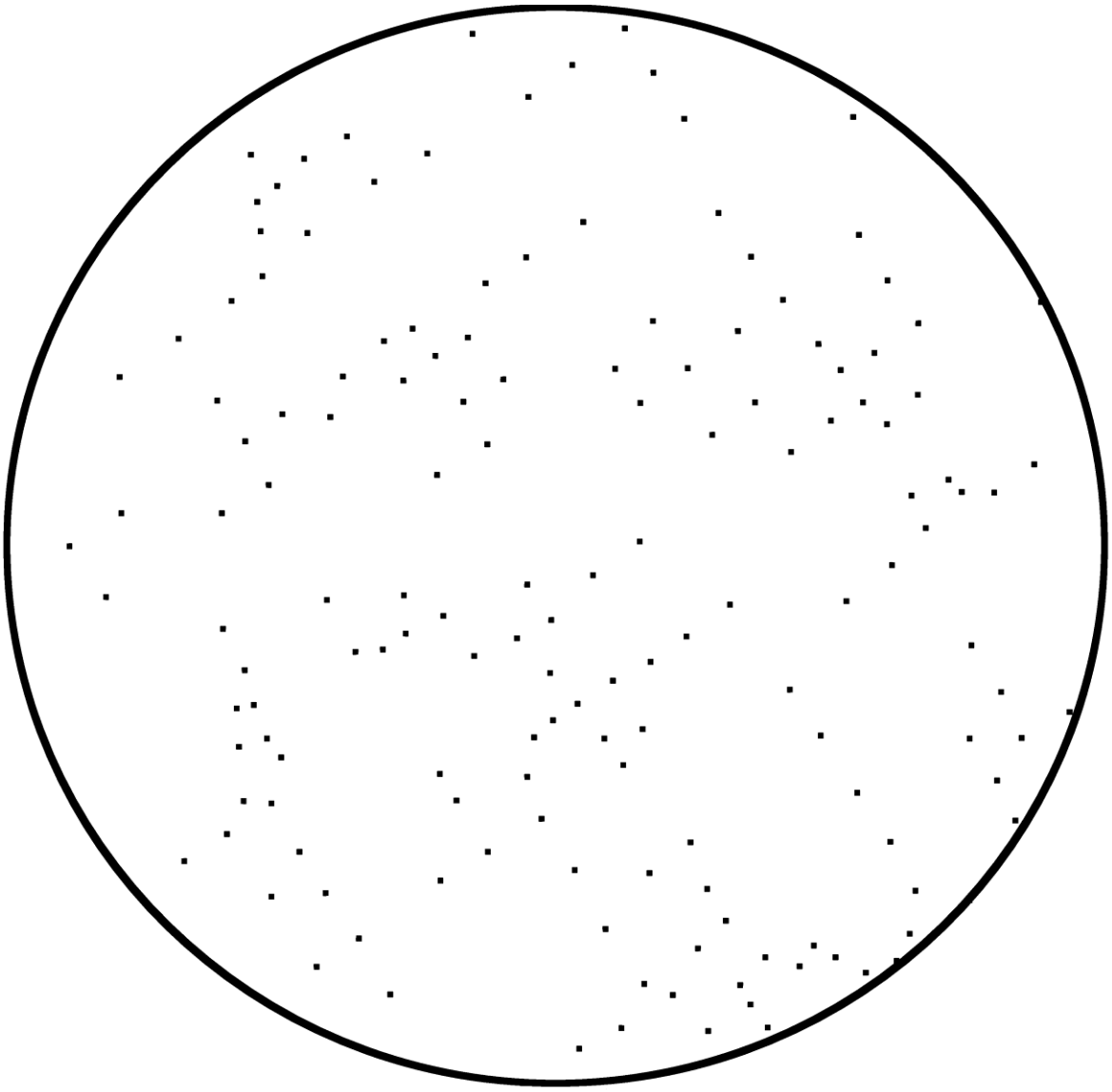

Figure 10. Distribution of dendrites, which was generated by Sigma scan pro software (as OV1 file) parallely while measuring X and Y, (dendrite centers) and the marks were of one pixel in size, the original image is dilated, altered for clarity.

2.5.2. Primary dendrite trunk diameter

Primary dendrite trunk-diameter was measured, using Sigma Scan Pro 4.0. Using the BMP image, “trace measurement options” was selected from “measure” menu, which displayed a window with available measurements to be added into the dialog box. “Distance” variable was selected and added into the dialog box. Then from the “tools” menu, “pixel pointer” of size one was selected and two perpendicular lines were drawn from one end to the opposite end of the dendrite trunk, as shown in the Figure 11 with red crosses. The width of these crosses (originally one pixel) has been enhanced for the sake of clarity. The soft-ware allowed the length and orientations of the two lines being drawn to be recorded in the Sigma Scan Pro worksheet. Average length of the two crosses is assumed to represent the individual primary dendrite trunk diameter.

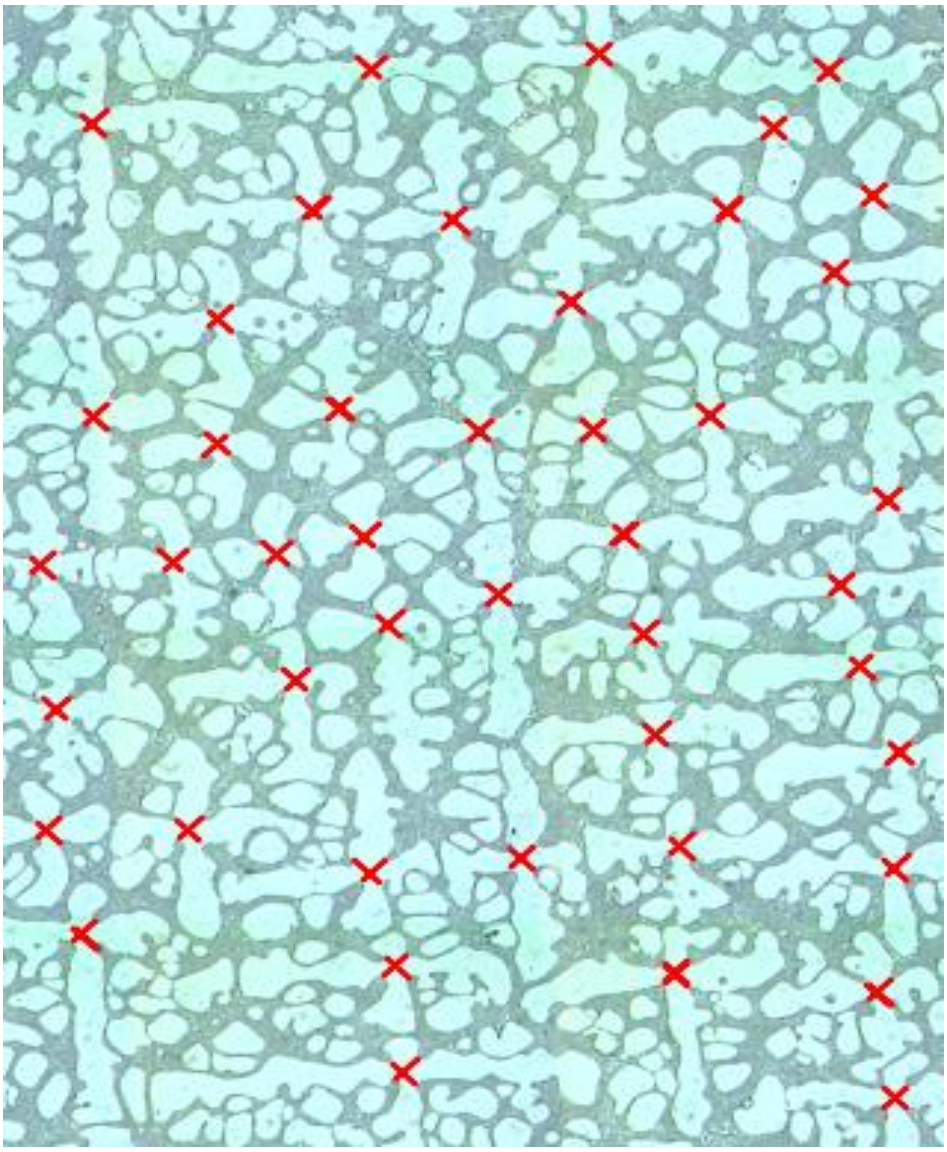

Figure 11. Measurement of primary dendrite trunk diameter of Al–7 wt% Si Alloy on its Transverse Microstructure obtained at Growth Velocity (R) =72 µm s^{-1} and Thermal Gradient = 40 K cm^{-1}.

2.5.3 Side branch length and side branching orientation

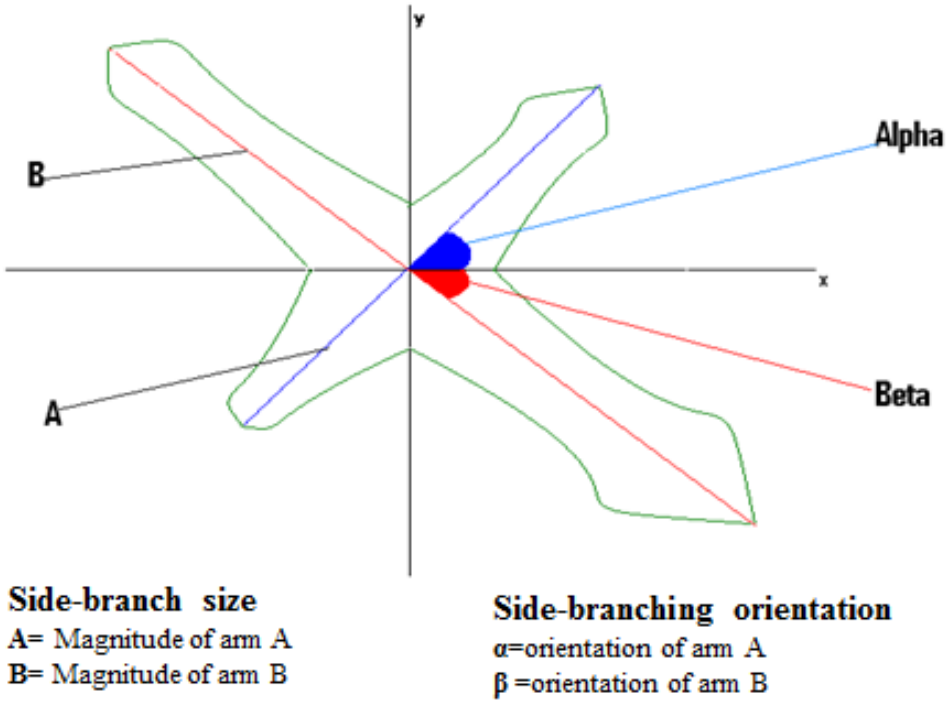

Figure 12. Measurement of magnitude and slope of side branches A and B which is shown by a manually drawn picture.

Sigma Scan Pro 4.0 was also used to measure the magnitude and orientation of the secondary dendrites (the side branches). Four parameters for every primary dendrite across the entire sample cross-section: the side branch length A and its orientation α, and the side branch B and its orientation (as schematically shown in Figure 12).

CHAPTER III

RESULTS AND DISCUSSION

Two Al-7 wt% Si alloy samples directionally solidified at 40 K cm^{-1} are used for this study, where different step increase and step decrease in growth speeds was introduced to examine their influence on the primary dendrite morphology and distribution. These samples were earlier examined by Ravi S Rajamure [10]. His thesis looked at microstructures during steady-state growth, i.e., when thermal gradient and growth speed are kept constant during directional solidification, mainly concentrating on the primary dendrite spacing measurements. In this research the emphasis is on another morphology parameter, the primary dendrite trunk diameter, and also examining the evolution of microstructure immediately after the growth speed step change, either a step decrease or a step increase.

Figures 13 (a) and (b), 11-13 and 11-18 respectively, show schematic views of the two directionally solidified bars that have been used for this study. The 11-13 sample (Figure 13(a)) was initially grown at 4.2 μm s^{-1} for 6.4 cm. Its speed was then increased to 85 μm s^{-1} and maintained for 8-cm, when the speed was decreased to 31 μm s^{-1} and

maintained for 6.2 cm. The rest of the sample was then rapidly pulled-out from the furnace. The 11-18 sample (Figure 13(b)) was initially grown at 72 μm s^{-1} for 7.3 cm. Then its speed was decreased to 4.85 μm $s^{-1}$and maintained for 6.7 cm, when is speed was increased to 22 μm s^{-1} and maintained for 6 cm before rest of the melt column being rapidly withdrawn from the furnace. As mentioned in the experimental procedure section, transverse microstructures were examined at about 3.8 mm steps along the length of the directionally solidified samples, except in the immediate vicinity of the speed-changes. Here 2-cm long pieces, with the speed transitions approximately located in the middle (1-cm location), were sliced-off. These were then examined at much closer steps, 300 – 500 μm, by serial sectioning and examination of transverse microstructures.

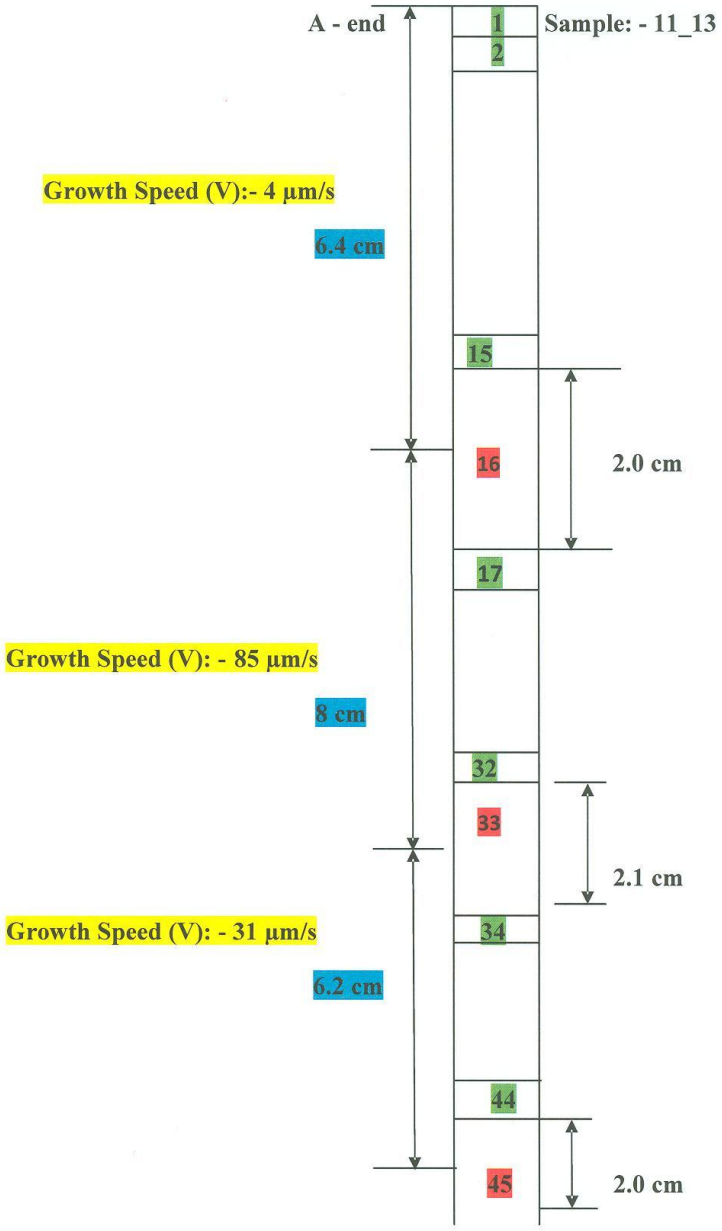

Figure 13(a): Schematic view of Al– 7 wt% Si alloy (11_13 Sample) which was directionally solidified at various growth speeds.

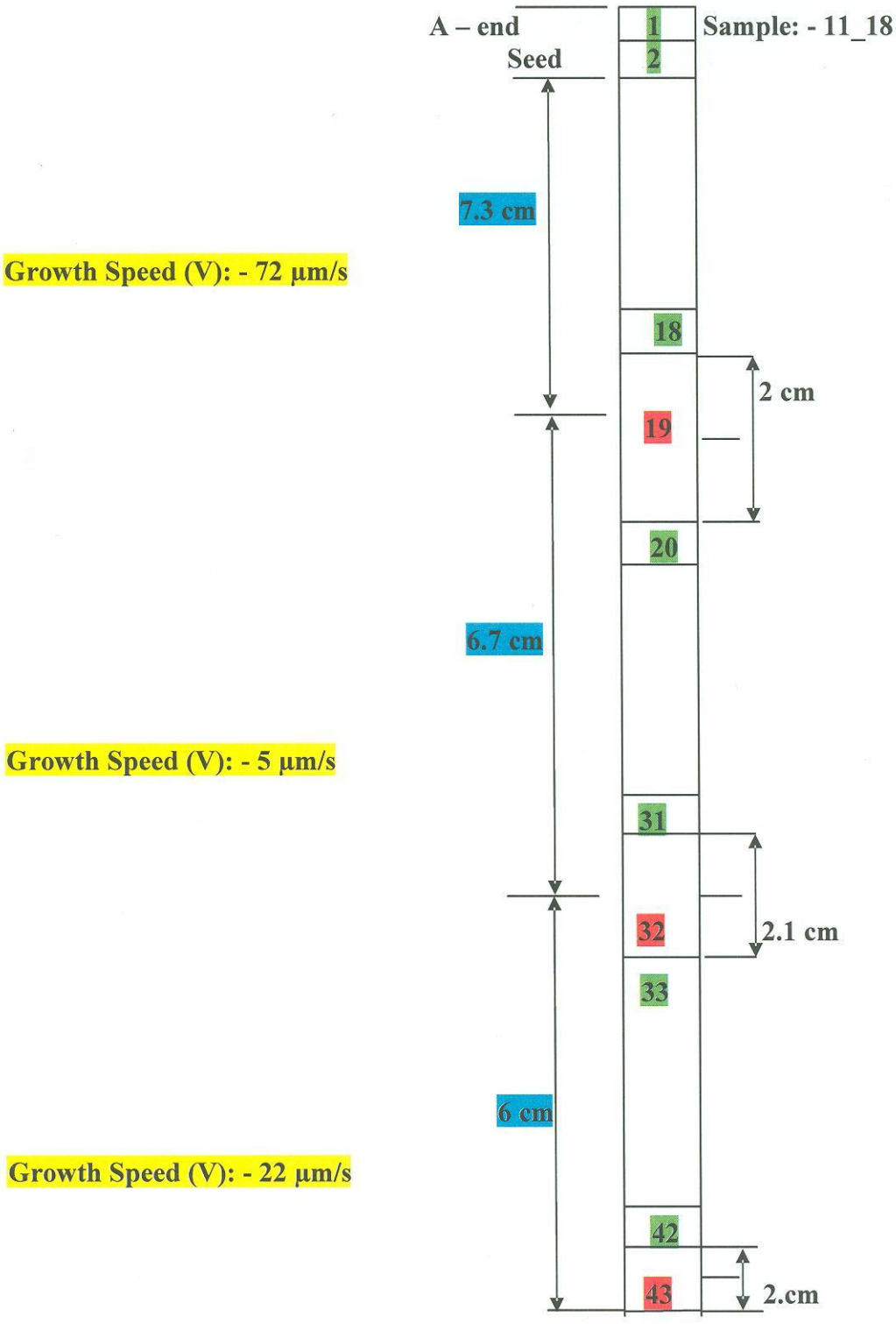

Figure 13(b): Schematic view of Al–7 wt% Si alloy (11_18 Sample) which was directionally solidified at various growth speeds.

3.1. Typical Transverse microstructures at various growth speeds

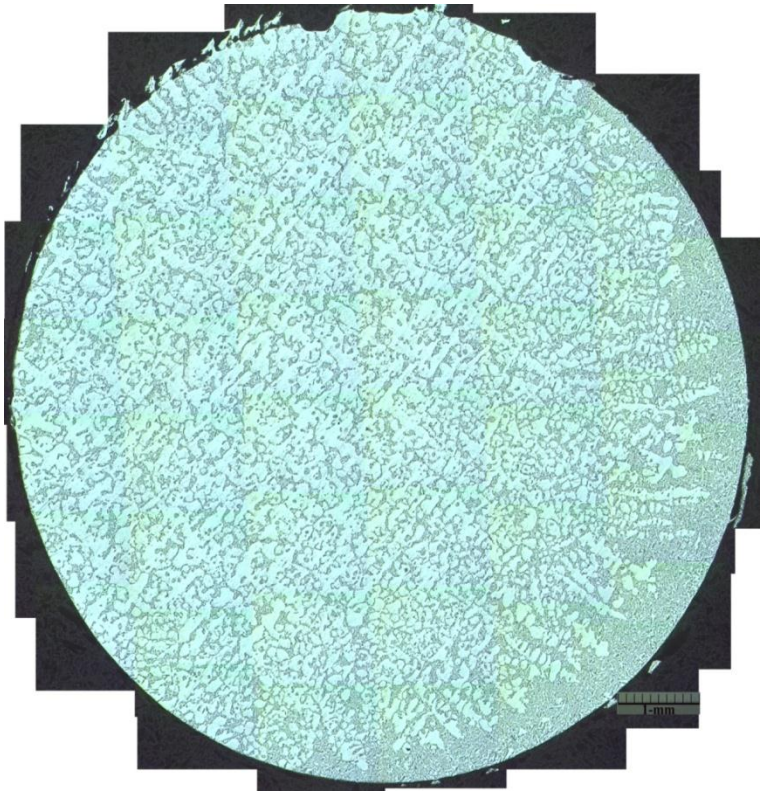

Figure 14. 11-18-29, transverse microstructure of an Al- 7 wt% Si alloy directionally solidified at 40 K cm^{-1}, 42 cm after the speed was reduced from 72 µm s^{-1} to 4.2 µm s^{-1}.

Figure 14 shows transverse microstructure (11-18-29) corresponding to a low growth speed of 4.2 µm s^{-1}, at a distance of 4.42 cm after the speed was decreased from 72 µm s^{-1}. There is significant dendrite clustering (dendrite steepling) at this speed- distribution of primary dendrites is not uniform across the sample cross-section causing significant transverse macro-segregation. The central portion has more primary dendrites, hence is aluminum rich, whereas the outer periphery has more Al-Si eutectic, hence, is silicon rich, as compared with the Al-7 wt% Si alloy composition. Also the primary dendrites are not well-branched at this low speed.

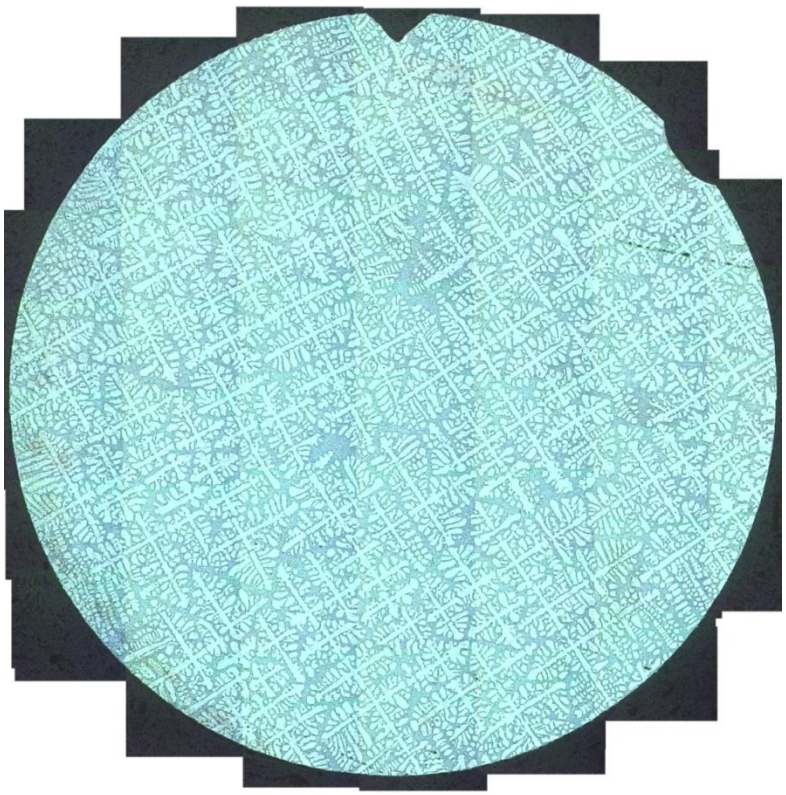

Figure 15. 11-13-44, transverse microstructure of Al-7 wt% Si alloy directionally solidified at 40 K cm^{-1}, 4.80 cm after the speed was decreased from 85 μm s^{-1} to 31 μm s^{-1}.

Figure 15 presents transverse microstructure (11-13-34) of a sample directionally solidified at intermediate growth speed 31 μm s^{-1}. This section was located at 4.80 cm after the speed was decreased from 85 μm s^{-1} to 31 μm s^{-1}. At this speed the "dendrite clustering" is absent; the primary dendrites are uniformly distributed across the entire sample cross-section. The secondary branches are well defined, and tertiary branches are clearly evident.

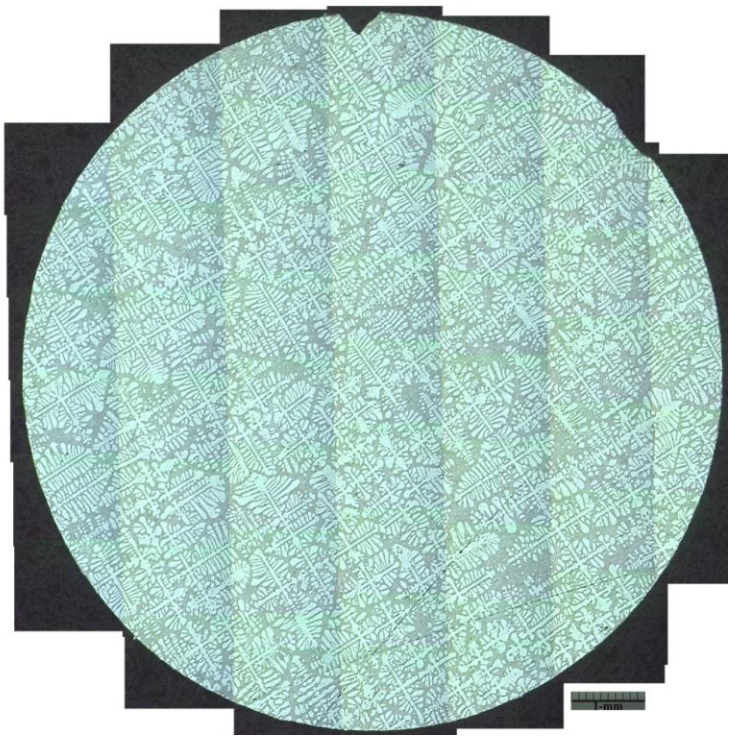

Figure 16. 11-13-32, transverse microstructure of Al-7 wt% Si alloy directionally solidified at 40 K cm^{-1} at 85 μm s^{-1} (microstructure 6.70 cm after the step increase from 4.2 μm s^{-1}).

Figure 16 presents transverse microstructure (11-13-32) for a high growth speed of 85 μm s^{-1}. This section was located at 6.70 cm after the speed was increased from 4.2 to 85 μm s^{-1}. At this higher growth speed, the primary dendrites are finer with smaller spacing as compared with those at 31 μm s^{-1}. In addition the dendrites are uniformly distributed across the sample cross-section without any indication of transverse macro-segregation.

3.2. Some important observations made on the directionally solidified Al-7 wt% Si alloy transverse microstructures during the transient after the step change in growth speed

3.2.1. Changes observed in the transverse microstructures after step decrease in growth speed from 85 to 31 μm s^{-1}

Table 2: Number of disappeared primary dendrites with respect to the distance after the during the transient within 2.1 cm distance

Sample ID	Translational distance, cm	No. of disappeared primary dendrite trees
11_13_33_1	0.038	0
11_13_33_10	0.291	0
11_13_33_20	0.569	6
11_13_33_30	0.889	6
11_13_33_40	1.192	2
11_13_33_50	1.493	5
11_13_33_58	1.738	4
11_13_33_60	1.798	3
11_13_33_68	2.075	3

During the Directional Solidification of Al-7 wt% Si alloy (G=40 K cm^{-1}), with the step decrease in the growth speed from 85 to 31 μm s^{-1}, it was observed that some of the primary dendrites are melting away while their neighboring dendrites are growing. Table 2 shows number of primary dendrite trees disappeared (melted) within the translational of distance of about 2.1 cm. Figure 17 shows the transverse microstructure, 11-13-33-10, with 29 colored primary dendrites and is located at 0.709 cm distance before the speed change. The colored primary dendrites are the ones which are disappearing slowly with the distance. Figure 18 shows transverse microstructure, 11-13-33-40, obtained at a distance of 0.192 cm after the speed change, fourteen trees are disappeared at this distance. The length of the side branches of the disappearing primary dendrite trees is decreased with distance after the speed change which is clearly seen in 11-13-33-40

(figure 18) when compared with same colored primary dendrite trees present in the transverse section, 11-13-33-01. (Figure 37) before the speed change.

Figure 18 has fifteen colored dendrites which are disappeared at a distance of 1.04 cm, which is seen in the transverse microstructure, 11-13-33-68, shown in figure 19.

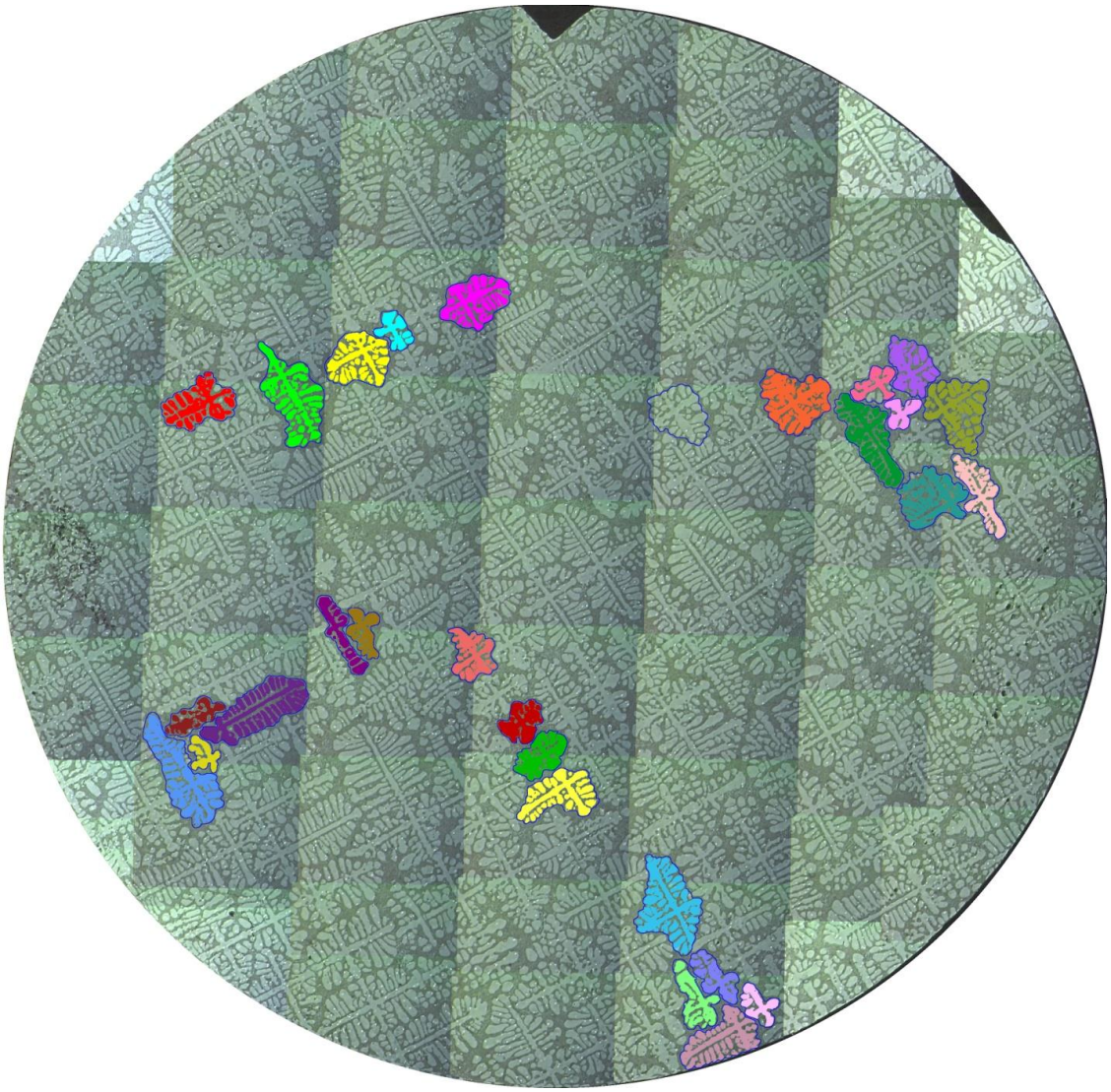

Figure 17. 11-13-33-10, transverse microstructure of an Al-7 wt% Si alloy, directionally solidified at 40 K cm^{-1}, after a speed decrease from 85 to 31 μm s^{-1},0.709 cm distance

before the speed change, 29 primary dendrite trees which are disappeared during the transient are colored.

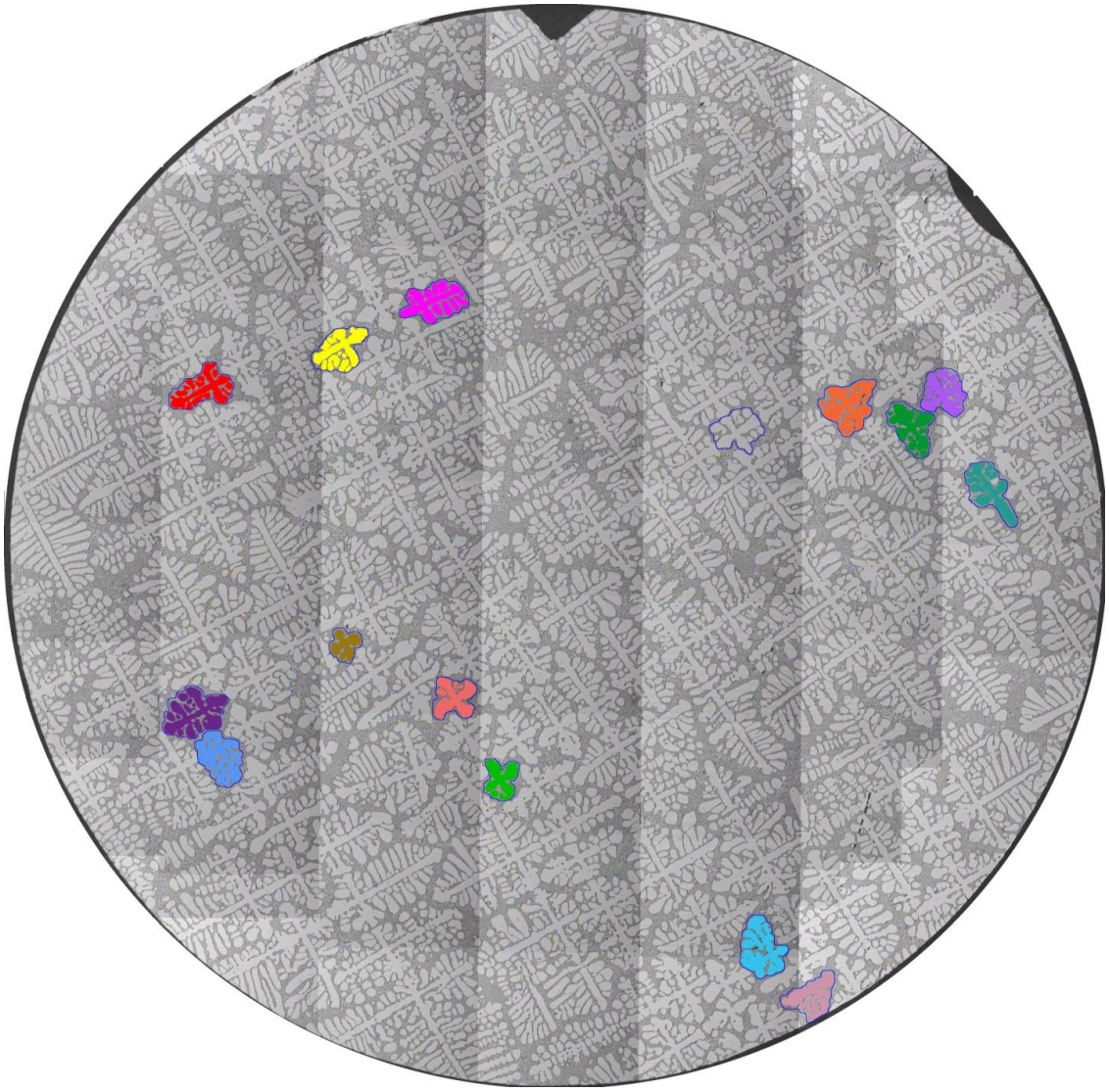

Figure 18. 11-13-33-40, transverse microstructure of an Al-7 wt% Si alloy, directionally solidified at 40 K cm^{-1}, at 0.192 cm distance after a speed decrease from 85 to 31 μm s^{-1}, 15 primary dendrites are melted away at this distance.

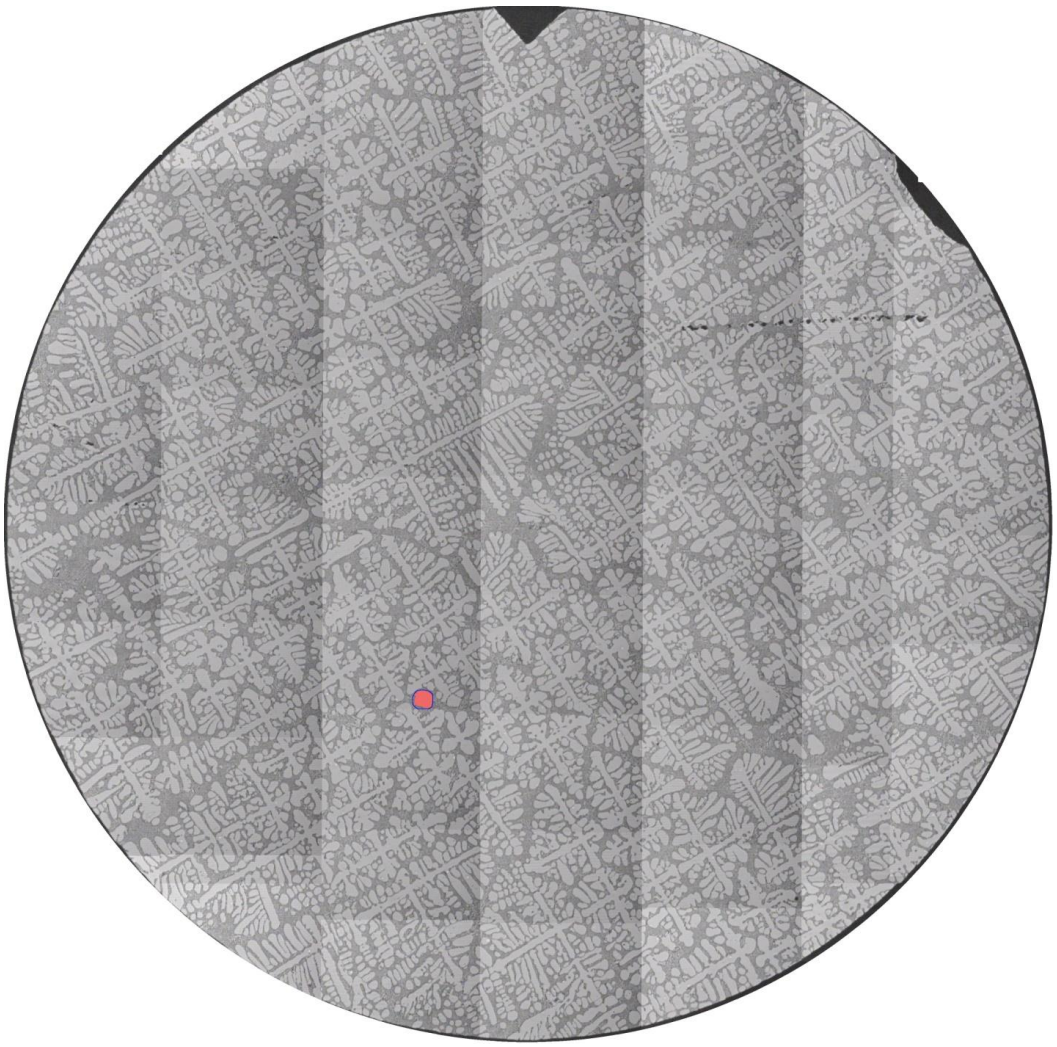

Figure 19. 11-13-33-68, transverse microstructure of an Al-7 wt% Si alloy, directionally solidified at 40 $Kcm^{-1,}$ at 1.04 cm distance after a speed decrease from 85 to 31 μm s^{-1}, all the colored primary dendrites are disappeared at this distance.

3.2.2. Changes observed in the transverse microstructures of Al- 7wt% Si alloy during the directional solidification after step increase in growth speed from 4 to 85 μm s^{-1}, G= 40 K cm^{-1}

After the speed is stepped up from 4 to 85 μm s^{-1} during the directional solidification of Al- 7wt% Si alloy, initially dendritic structures are observed in the transverse sections, primary dendrites at the periphery of the transverse sections are observed to have very large side-arms protruded out which are seen clearly in figure 21 (11-13-16-34) which is at a distance of 0.05 cm before the speed change. After some distance, very large side arms of these primary dendrite trees at the periphery of the transverse section were broken into many small fragments which are grown as individual dendrite trees which could be seen in the figure 22, 11-13-16-43 at 0.28 cm after the speed change. It is also observed that dendrites in the center of the transverse section had grown at consistent length and no fragmentation is observed in these trees. Figure 23 shows the transverse microstructure (11-13-16-63) of Al-7 wt % Si alloy directionally solidified at 40 K cm^{-1} obtained at 0.89 cm distance after the step change in growth speed from 4.2 to 85 μm s^{-1} with uniform dendrite distribution (64 transverse sections were carefully polished at incremental distance to obtain microstructures for statistical analysis)

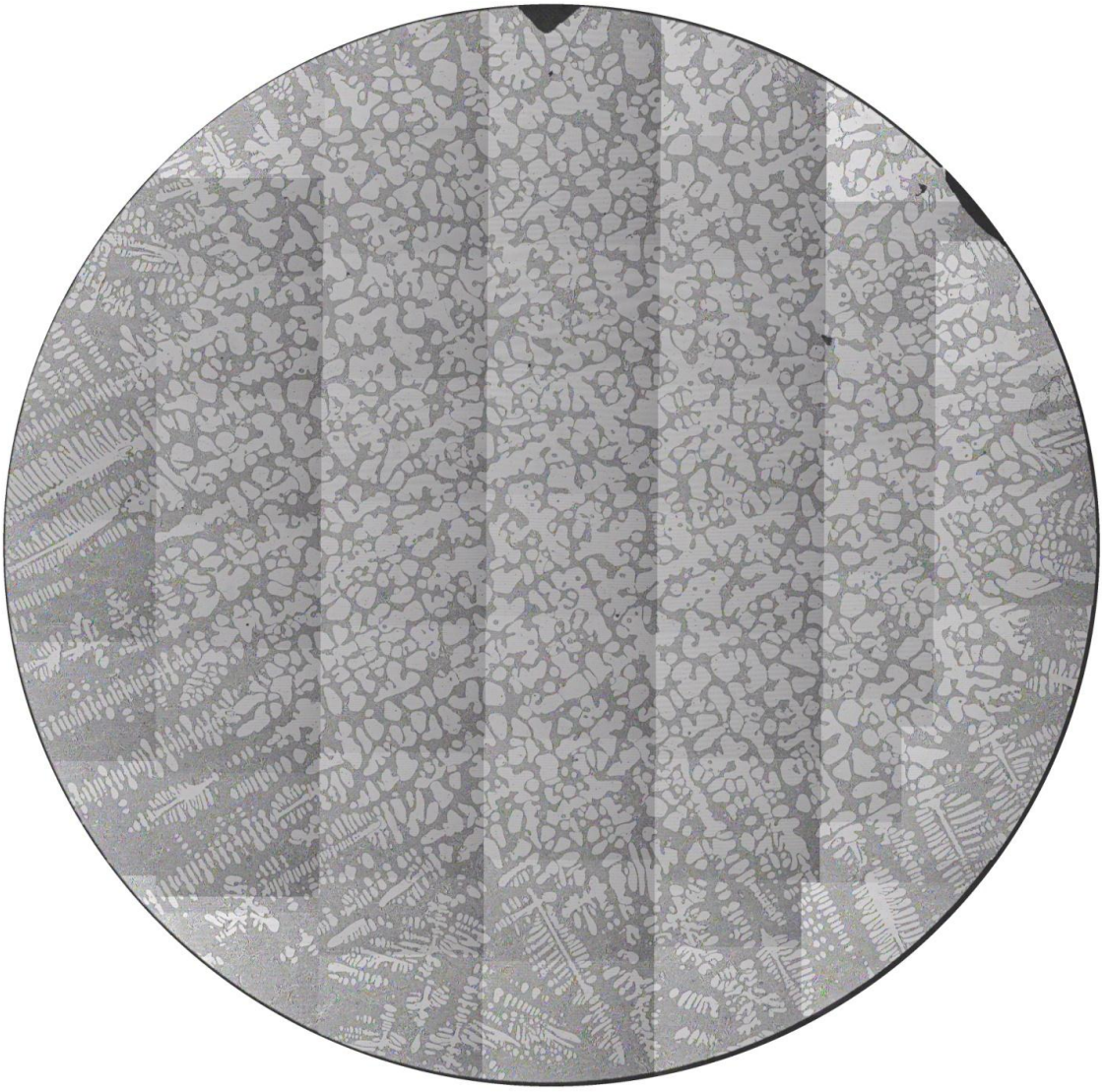

Figure 20. (11-13-16-23), transverse microstructure of Al-7 wt % Si alloy directionally solidified at 40 K cm^{-1}, at 4.2 μm $s^{-}1$ before the step increase in growth speed.

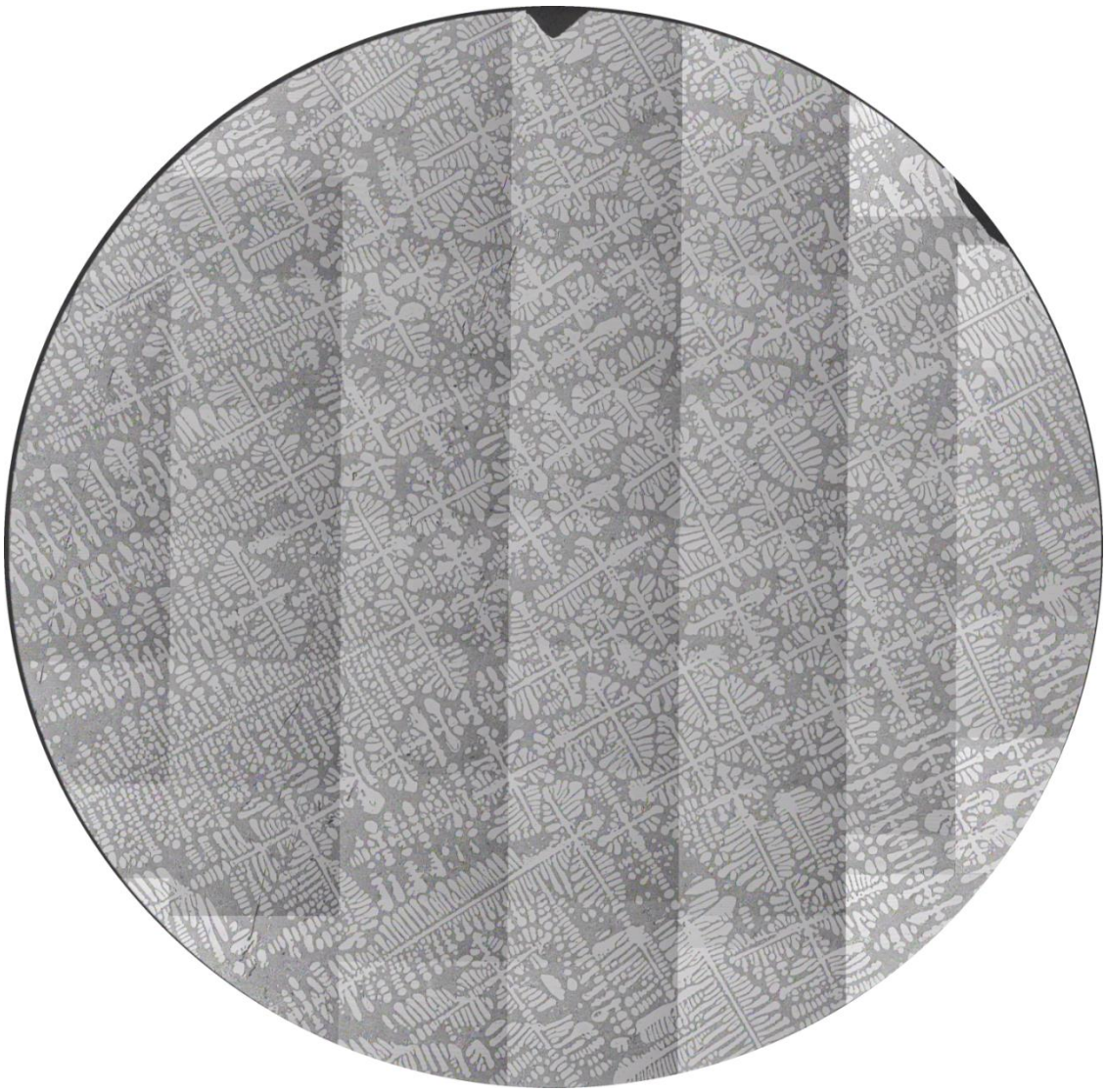

Figure 21. (11-13-16-34), transverse microstructure of Al-7 wt % Si alloy directionally solidified at 40 K cm^{-1}, 0.02cm distance after the step increase in growth speed from 4.2 to 85 μm s^{-1}.

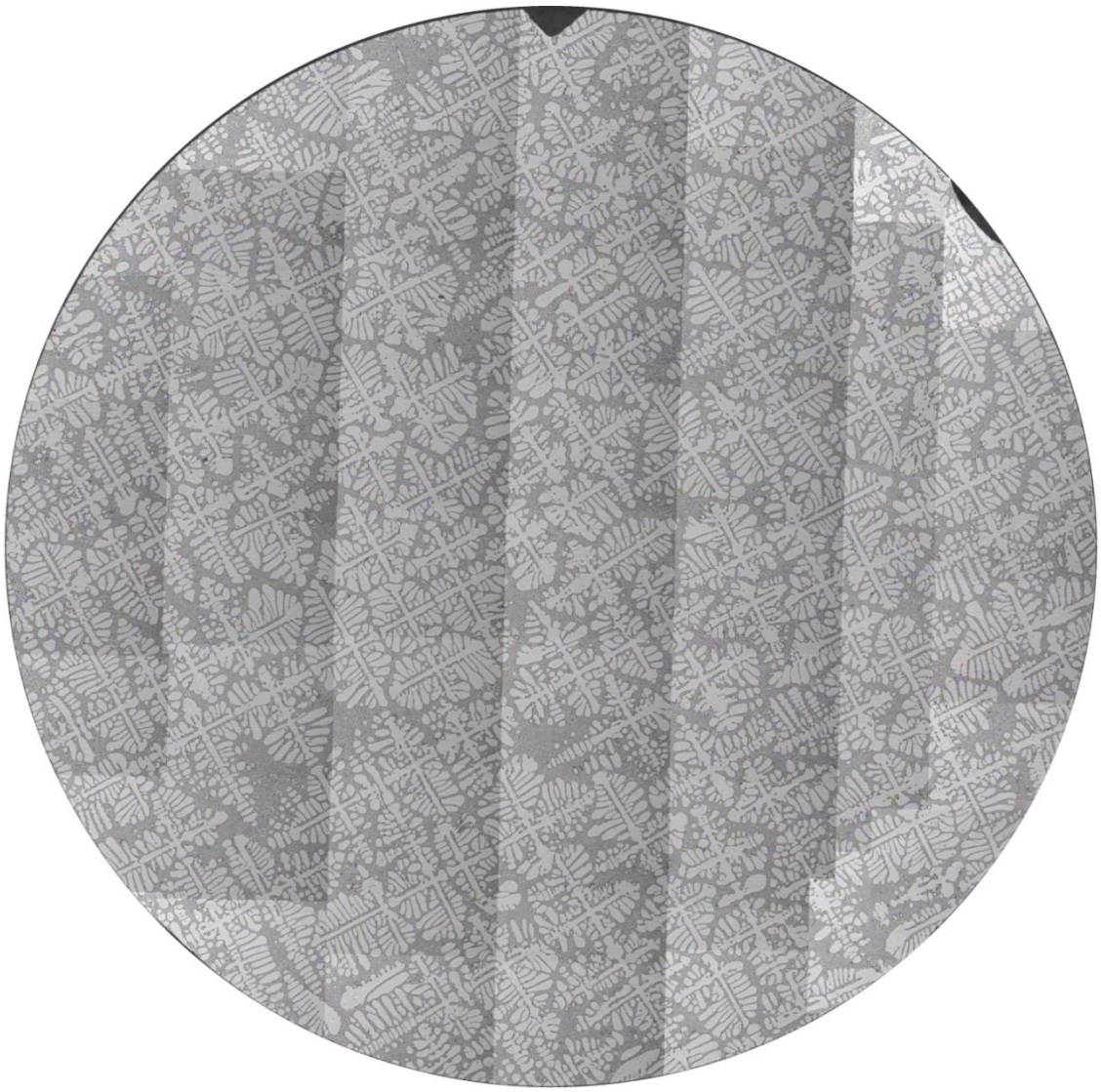

Figure 22. (11-13-16-43), transverse microstructure of Al-7 wt % Si alloy directionally solidified at 40 K cm^{-1}, 0.28 cm distance after the step increase in growth speed from 4.2 to 85 μm s^{-1}.

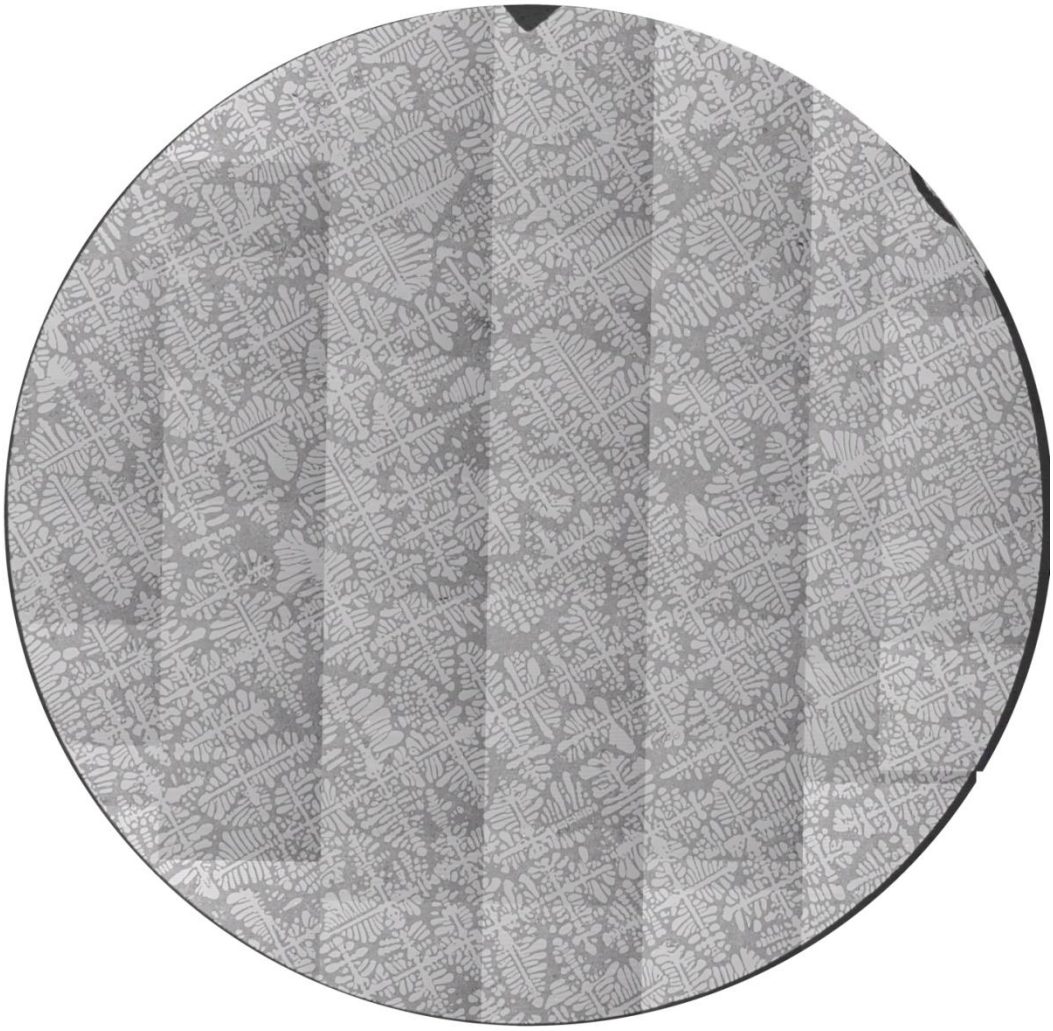

Figure 23. (11-13-16-63), transverse microstructure of Al-7 wt % Si alloy directionally solidified at 40 K cm^{-1}, 0.89 cm distance after the step increase in growth speed from 4.2 to 85 μm s^{-1}.

3.3. Growth speed dependence of primary dendrite trunk diameter

Figure 24 shows the growth speed dependence of primary dendrite trunk diameter for the Al-7 wt% Si alloy directionally solidified at 40 K cm^{-1}. It plots the mean and the standard deviation values. It also includes the primary dendrite nearest neighbor spacing for comparison. Both the primary dendrites spacing and the trunk diameter shows a decrease with increasing growth speed. The decrease in the primary spacing appears to be steeper than that in the trunk diameter, and also the relative scatter in the spacing appears to be larger than that for the spacing.

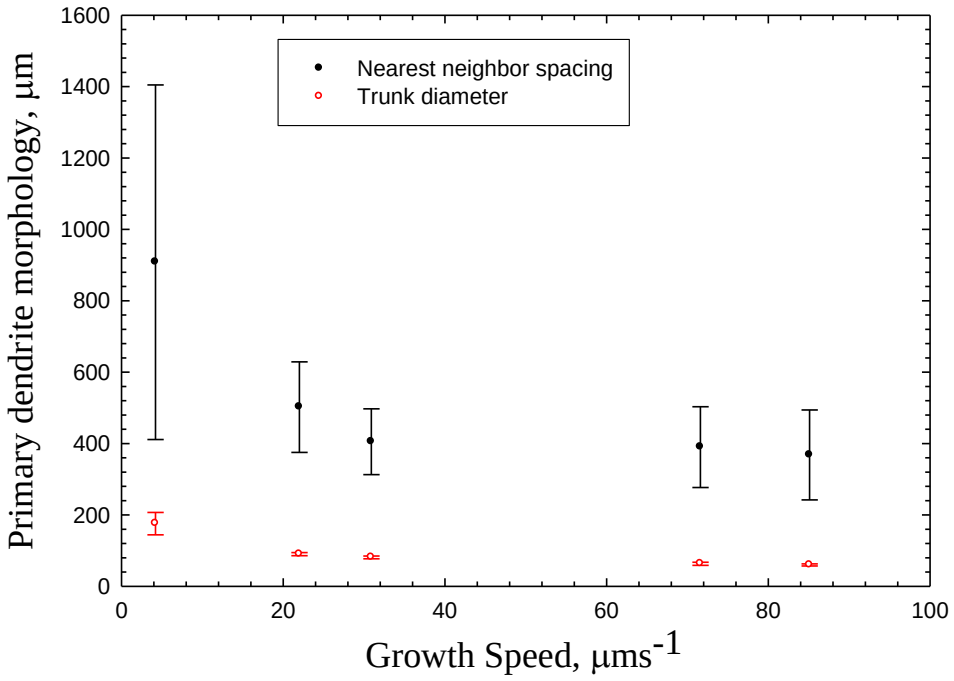

Figure 24. Correlation of Growth speed dependence of primary dendrite trunk diameter and nearest neighbor spacing for an Al- 7 wt % Si alloy, directionally solidified at 40 K cm^{-1}.

Figure 25 plots the ratio of the standard deviation to mean for the trunk diameter and the nearest neighbor spacing for various growth speeds. It confirms the observation that relative noise in the distribution of the nearest neighbor spacing is significantly larger than that in the trunk diameter, suggesting that trunk diameter may be a more insightful feature to identify changes introduced by small changes in any processing parameters, such as those introduced by natural convection or its absence.

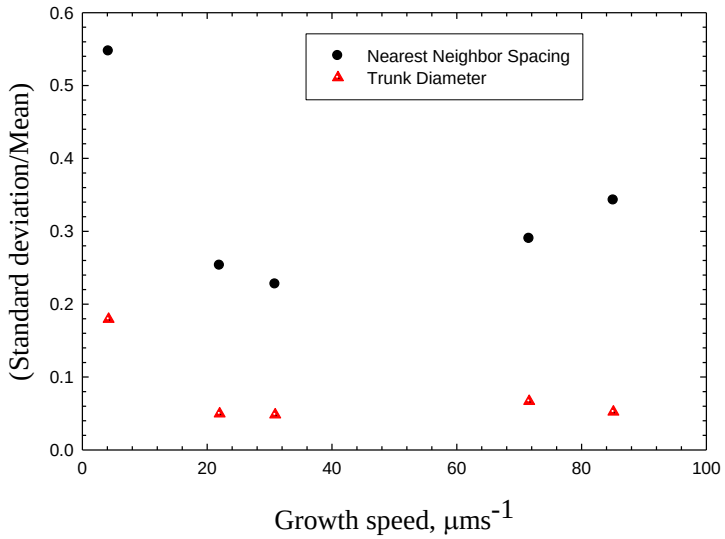

Figure 25. Ratio of the standard deviation to mean for the nearest neighbor spacing and primary trunk diameter plotted as a function of growth speed for an Al- 7 wt % Si alloy, directionally solidified at 40 K cm^{-1}.

Figure 26 plots the growth speed dependence of the ratio of the nearest neighbor spacing to the primary trunk diameter for an Al-7wt%Si alloy directionally solidified at 40 Kcm^{-1}. The broken line is the linear least square regression fit to the experimental data. This

figure shows that the ratio of nearest neighbor spacing to trunk diameter increases with increasing growth speed.

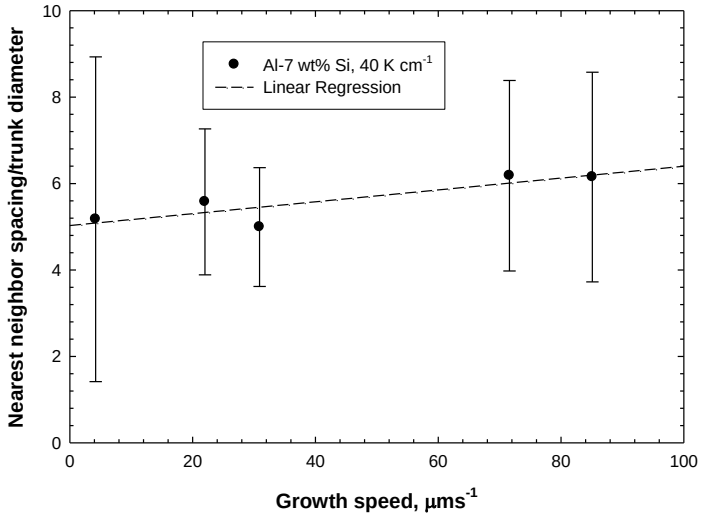

Figure 26. Growth speed dependence of ratio of nearest neighbor spacing to dendrite trunk diameter of an Al-7wt%Si alloy, directionally solidified at 40 K cm^{-1}.

Since the tips of dendrites are parabolloidal in shape, at the tip the trunk diameter will be about twice the dendrite tip radius. However, it is expected to increase along the length of primary dendrites into the mushy zone both because of increased fraction solid formed and also by the surface energy driven coarsening where the nearby smaller curvature features, such as, tertiary branches will dissolve and the larger curvature feature (such as trunk diameter) will grow at their expense. This would suggest that the dendrite trunk diameter may be related to the dendrite tip radius. Since the theoretical solidification models predict that for a given thermal gradient and alloy composition the dendrite tip radius decreases with increasing growth speed [11], the trunk diameter is also expected to decrease with increasing growth speed. Figure 27 compares the experimentally observed

trunk diameter with the theoretically predicted dendrite tip radii [12]. The decreasing trend of the trunk diameter is similar to the decreasing trend of the predicted dendrite tip radius. However, the decrease in the trunk diameter is steeper.

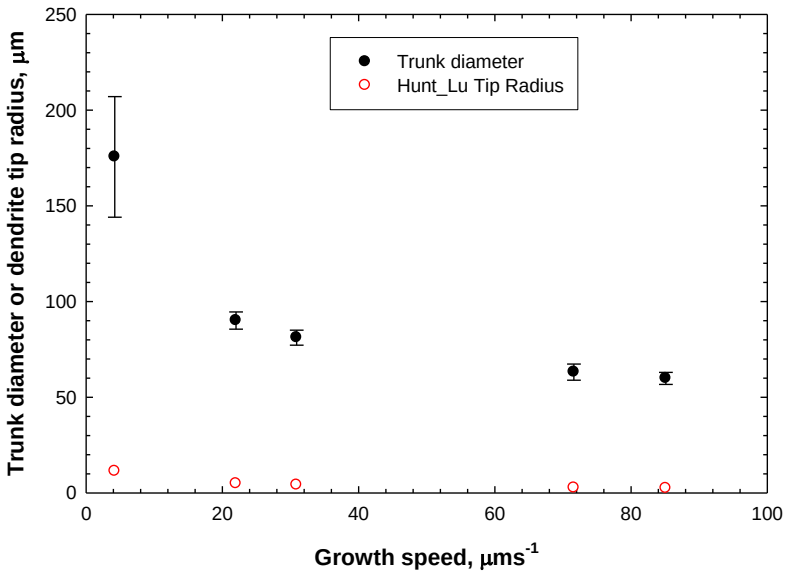

Figure 27. Experimentally observed trunk diameter and the theoretically predicted tip radii Hunt-Lu [12] for Al-7 wt % Si directionally solidified at 40 K cm^{-1}.

Table 3: Predictions from the Hunt-Lu model for dendrite array (Al- 7 wt% Si alloy, 40 K cm^{-1})

V (µm s^{-1})	1-s*	Tip radius (µm)	Tip comp (wt % Si)	Primary spacing (µm)
4.20	0.928	11.3	1.40	434
22.0	0.936	4.8	1.39	132
30.9	0.937	4.0	1.40	103
71.6	0.938	2.6	1.43	56
85.1	0.938	2.4	1.43	49

The effective thermal gradient of 0.002732 is used.

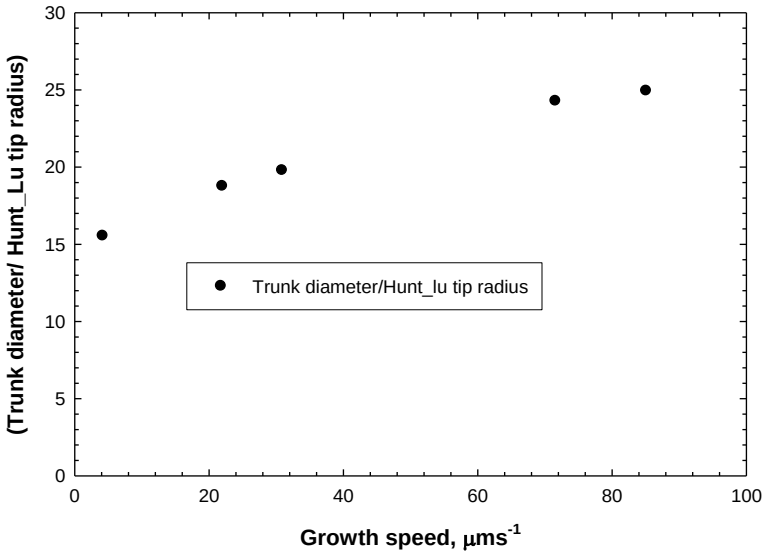

Figure 28. Ratio of experimentally observed mean trunk diameter to the theoretically predicted Hunt-Lu tip radii versus growth speed.

Figure 28 plots the ratio of the experimentally observed trunk diameter to the predicted Hunt-Lu [12] tip radii as a function of growth speed. It shows that with increasing growth speed the ratio of the trunk diameter to the predicted tip-radius decreases.

3.4. Primary trunk diameter change immediately after a step increase or the step decrease in growth speed

Figure 29plots trunk diameter as a function of distance over nearly 2-cm length. The initial 1-cm distance corresponds to the morphology at the previous speed (i.e., 4 μm s^{-1}) and the final 1-cm distance corresponds to the morphology after the speed change (i.e., 85 μm s^{-1}). The trunk diameter decreased from its value of 175 μm at 4 μm s^{-1} (Figure 20) to about 68 μm corresponding to the higher speed of 85 μm s^{-1} over a relatively short distance of about 2-mm after the a step change in speed. The decrease appears to start before the 1-cm location (the location which corresponds to the speed change) because

the liquid-solid interface is not one constant temperature, instead solidification occurs over a mushy zone length. For a thermal gradient of 40 K cm^{-1} and the alloy freezing range (liquidus-eutectic temperature) of 37 K, the mushy zone is about 1-cm long. The 2-mm distance for the trunk diameter to change is significantly smaller than the 4-cm of directional solidification length required for the nearest neighbor spacing to reach its new steady-state observed by Ravi [10]. This is shown in the Figure 30 [10].

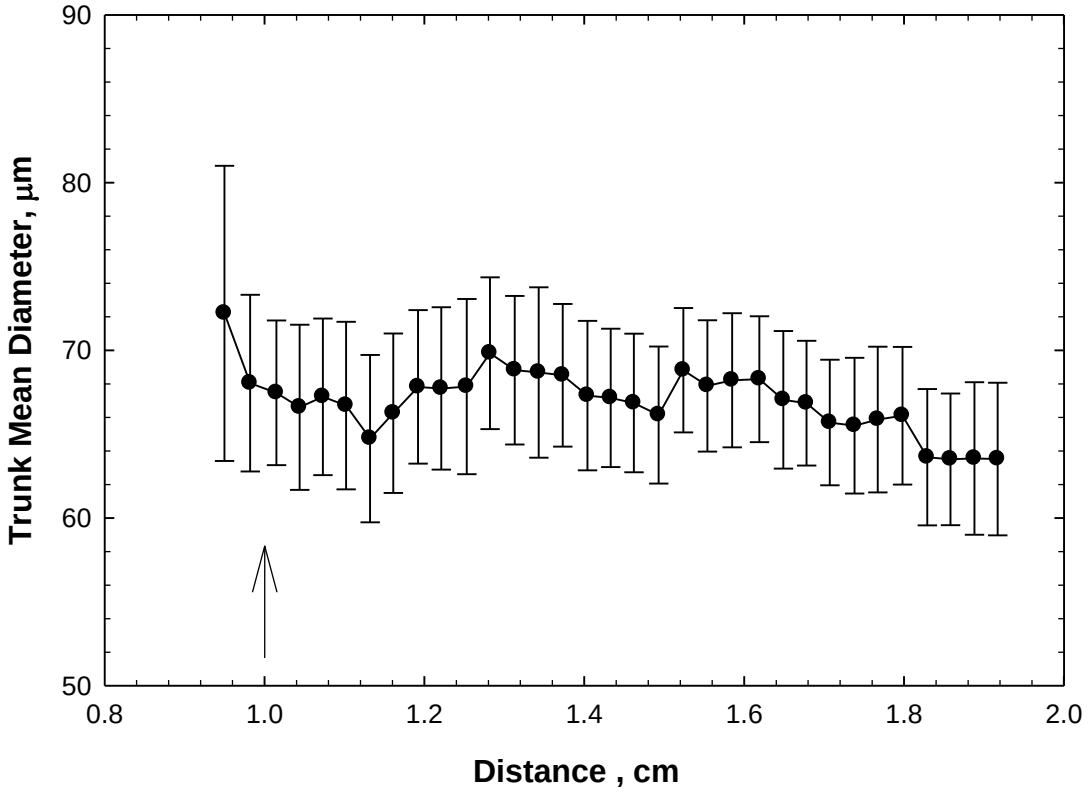

Figure 29. Trunk mean diameter during the transient after the step increase in growth speed from 4 to 85 μm s^{-1} of an Al –7 wt% Si alloy, directionally solidified at 40 K cm^{-1}.The data corresponds to the samples: (11-13-16-32 to 11-13-16-64).

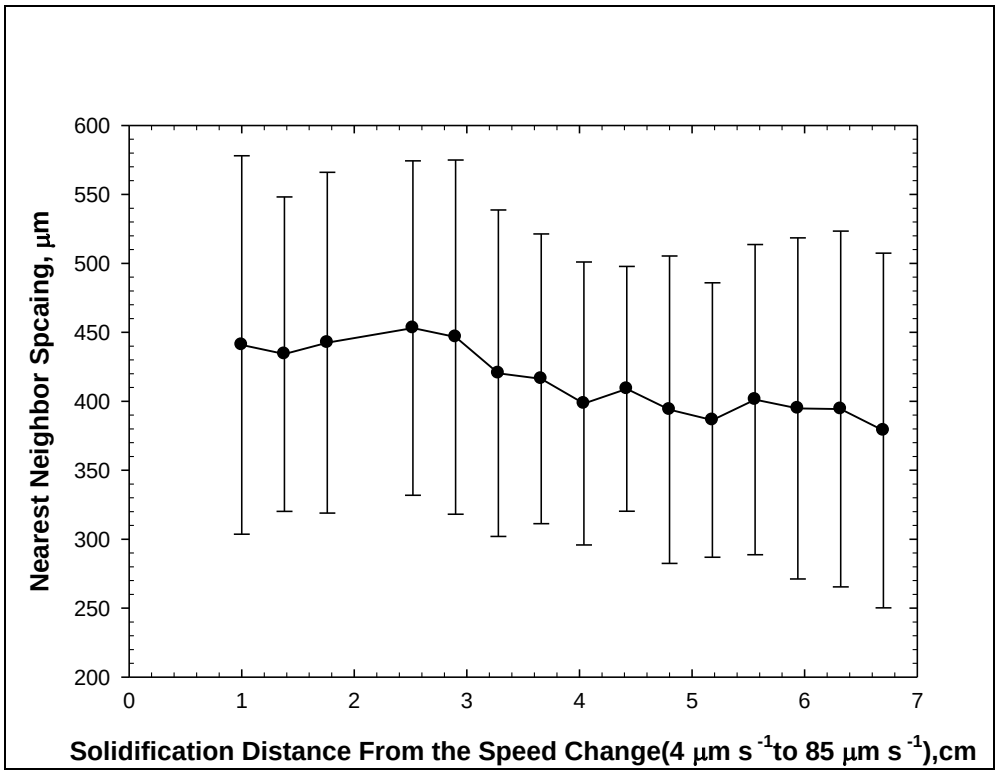

Figure 30. Nearest neighbor spacing after the step increase in growth speed from 4 to 85 μm s^{-1} during directional solidification of an Al–7 wt pct Si Alloy at thermal gradient of 40 K cm^{-1}. (The data corresponds to the samples: (11_13_17 to 11_13_32).

Figure 31 shows the variations in the trunk diameter after the step decrease in the growth speed from 85 to 31 μm s^{-1}. This figure also shows that the trunk diameter begins to increase about 1-cm before the onset of externally imposed speed change (the 1-cm location in this figure), and achieves its new steady-state value in much shorter distance as compared with the translation distance required for the nearest neighbor spacing to achieve its new distribution, about 3.5 cm, as observed by Ravi [10] (also plotted here in Figure 32 [10].

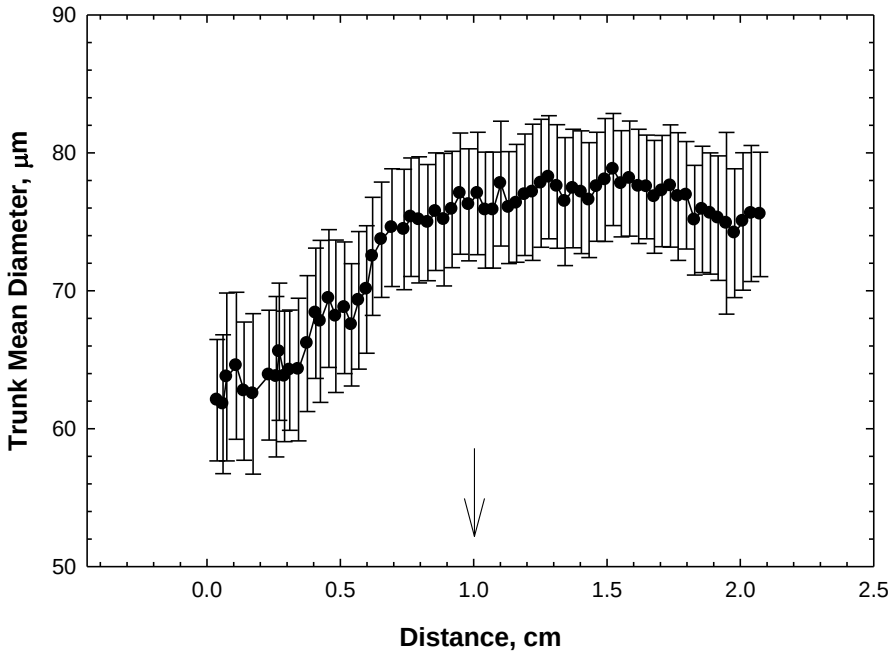

Figure 31. Trunk diameter during the transient after the step decrease in growth speed from 85 to 31 µm s-^{1} for an Al-7 wt% Si alloy directionally solidified at 40 K cm^{-1}. The data corresponds to the samples: (11-13-33-1 to 11-13-33-69).

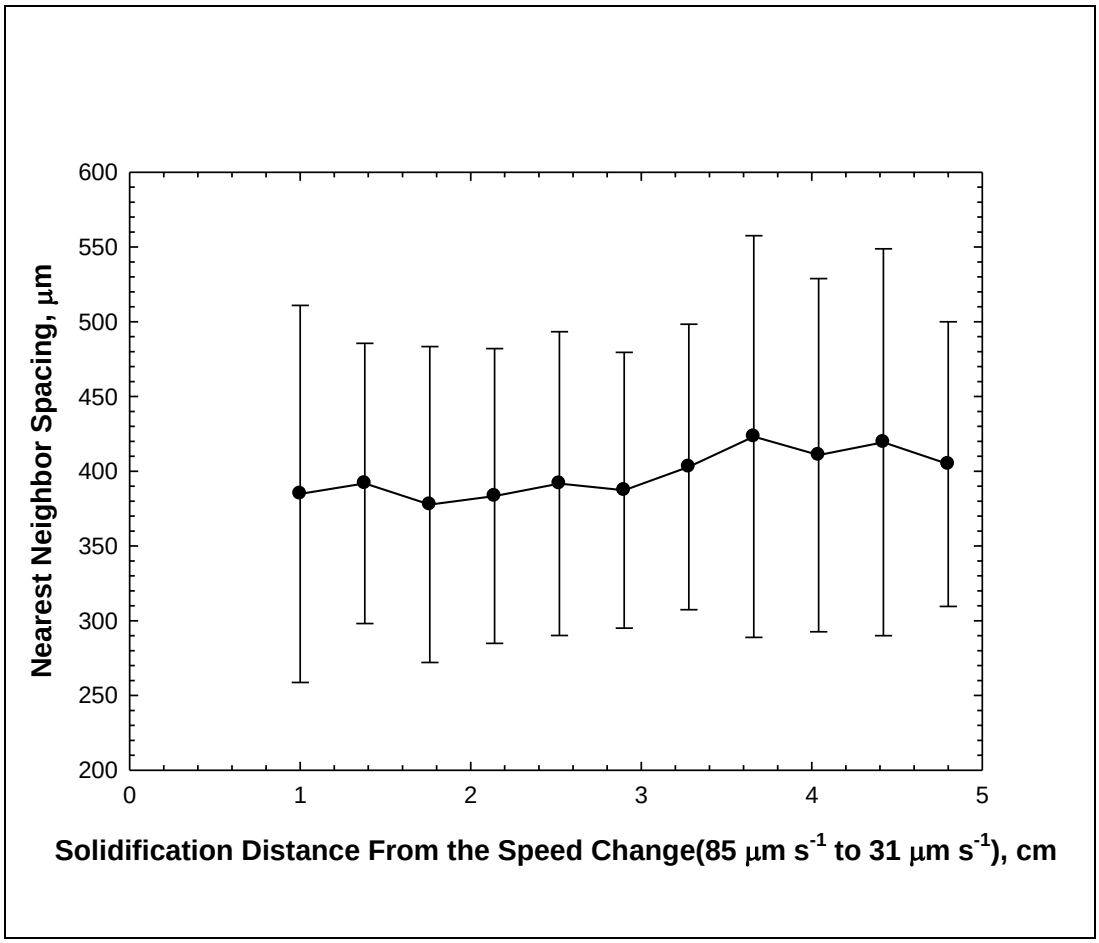

Figure 32. Neighbor Spacing distribution after the step decrease in growth speed from 85 to 31 μm s^{-1} , during directional solidification of Al – 7 wt pct Si at 40 K cm^{-1} (The data corresponds to the samples: (11_13_34 to 11_13_44).

3.5. Comparison of relative scatters in nearest neighbor spacing and in trunk diameter during the speed introduced transient and during steady-state growth

Figure 33 plots the ratio of standard deviation to mean of nearest neighbor spacing as a function of growth speed. The open symbols correspond to the steady-state growth regime (after more than 5-cm after the speed change), and the filled symbols correspond to the transient regime (1-cm after the speed change). The upwards and downwards

arrows correspondingly indicate growth speed increase and decrease steps, respectively. This figure indicates that the relative scatter in the nearest neighbor spacing during growth speed introduced transient is larger than that observed during steady-state arrayed growth of primary dendrites.

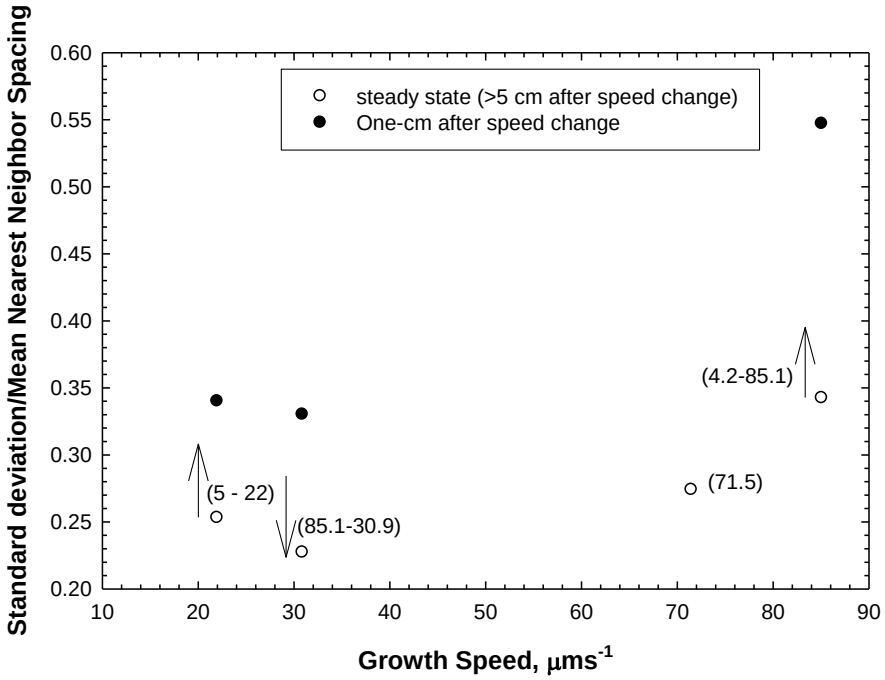

Figure 33. Ratio of standard deviation to mean of nearest neighbor spacing for an Al- 7 wt % Si alloy, directionally solidified at 40 K cm-1 at various growth speeds.

A similar behavior is also observed for the dendrite trunk diameter (Figure 34). However, the relative scatter in the trunk diameter is significantly smaller than that in the nearest neighbor spacing.

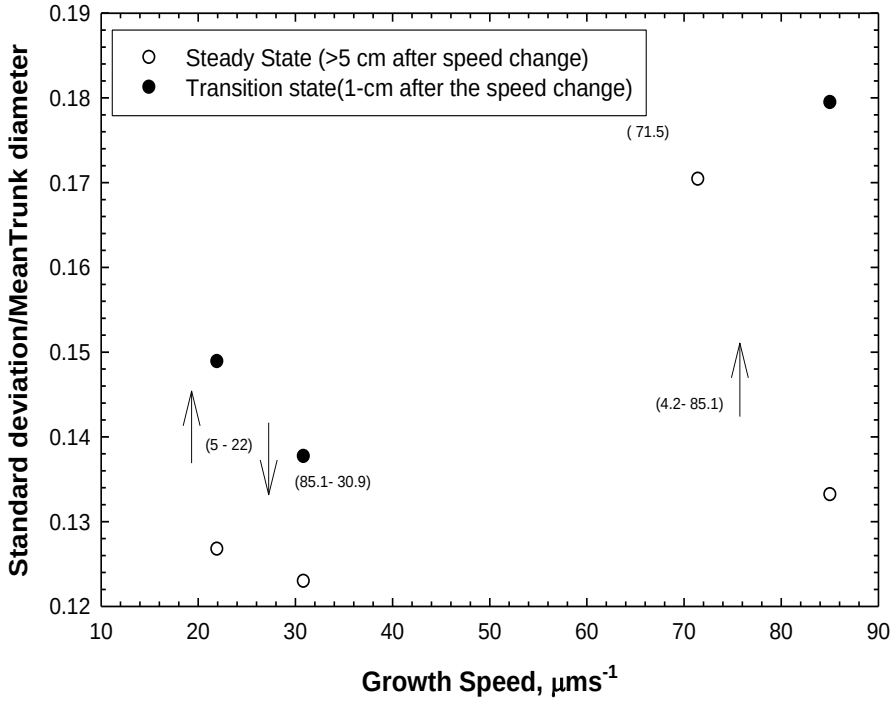

Figure 34. Ratio of standard deviation to mean for trunk diameter in an Al- 7 wt% Si alloy directionally solidified at 40 K cm^{-1} at several growth speeds.

3.6. Side-branch orientation (α-β), after step increase or after step decrease in growth speed

11-13-16(32:64)

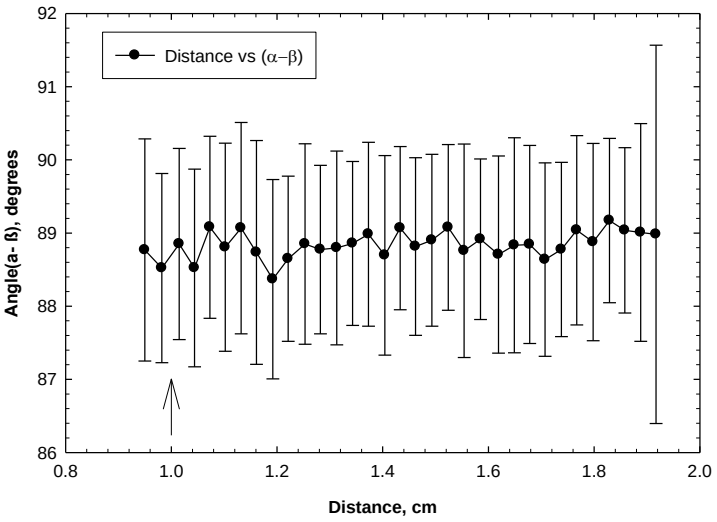

(a)

11-13-33, 85mms^{-1} - 30.9mms^{-1}

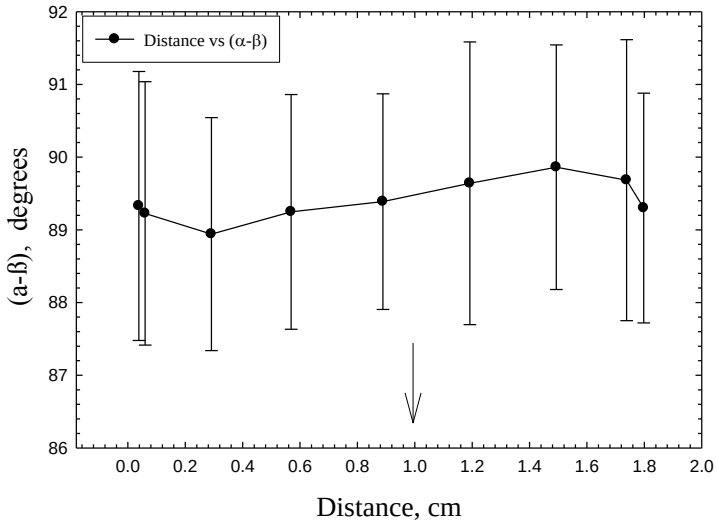

(b)

Figure 35. Side branch orientations of the primary dendrites during the transient after a sudden growth speed change (at 1-cm location) of an Al-7 wt% Si alloy, directionally solidified at 40 K cm^{-1}. (a) Growth speed increased from 4.2 to 85.1 μm s^{-1} and (b) Growth speed decreased from 85.1 to 30.9 μm s^{-1}.

Figure 35 presents the mean of side branch orientation of primary dendrites measured for an Al-wt% Si alloy sample during the transient after a sudden change in the growth speed's with respect to the solidification distance. The speed change corresponds to a distance of 1-cm in these plots. Figure 35 (a) shows the side branch orientation (α-β) after growth speed was increased from 4.2 to 85.1 μm s^{-1} and Figure 35 (b) shows the side branch orientation (α-β) after step decrease from 85.1 to 30.9 μm s^{-1}. The side branches remained oriented nearly normal to each other ((α-β) ~ 90^{o}) after the step-increase or the step-decrease in growth speed.

3.7. Side-branch length (A+B)/2, after step increase and after step decrease in growth speed

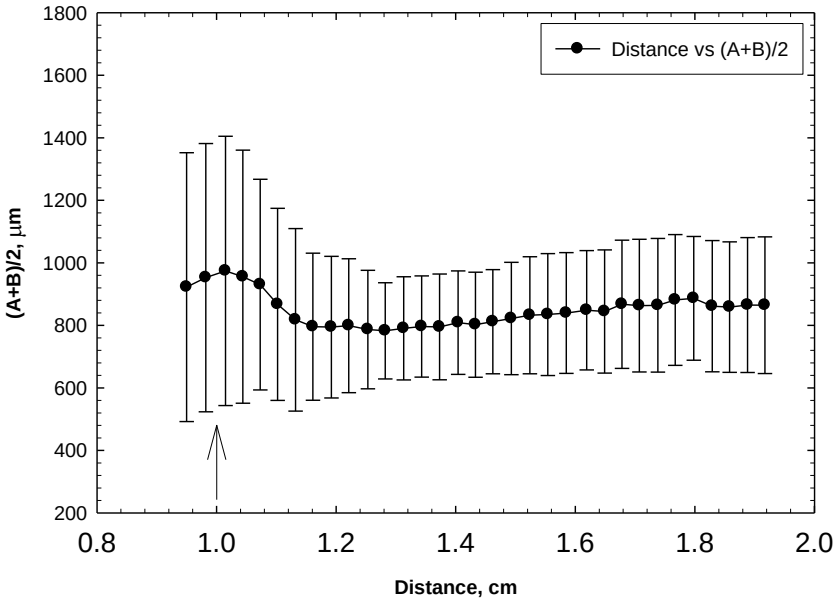

(a)

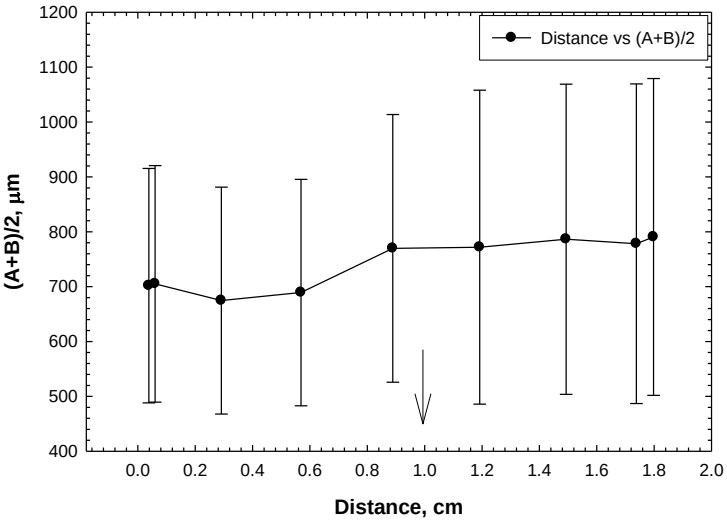

(b)

Figure 36. Average side branch length of the primary dendrites during the transient after a sudden growth speed change of an Al-7 wt% Si alloy, directionally solidified at 40 K cm^{-1}.

(a) Growth speed increased from 4.2 to 85.1 μm s^{-1} and (b) Growth speed decreased from 85.1 to 30.9 μm s^{-1}.

Figure 36 presents the mean side branch length, (A+B)/2, of primary dendrites during the transient after a sudden change in the growth speed. The change in speed corresponds to 1-cm mark in these figures. Figure 36 (a) is for increase in growth speed from 4.2 to 85.1 μm s^{-1} and Fig. 36 (b) corresponds to a speed decrease from 85.1 to 30.9 μm s^{-1}. These figures suggest that the mean side branch length begins to change about 2 to 6 mm before the externally imposed speed change location, and then they remain constant after that. Considering that mushy zone length is about 1-cm for these samples, this observation suggests that the length of secondary branches is determined within the 2 to 6-mm distance from the array tips, and perhaps during rest of the mushy zone length the side-branches only coarsen and do not become any longer.

3.8. The likely-hood of its survival or disappearance after a step decrease in the growth speed

It is well known that during arrayed growth of primary dendrites there exists a distribution in their morphologies, such as nearest neighbor spacing, trunk diameter, secondary branch orientation and secondary-branch size. It is also known that step decrease in growth speed causes some of the primary dendrites to melt-away while their neighboring dendrites grow in size and thus a decreased neighbor spacing is achieved at

lower growth speed. However, it is not known which of these morphologies are responsible for determine the fate of a typical dendrite in an array.

Figure 37 shows in color several primary dendrites which were observed to slowly disappear over a transition distance of about 2.1 cm during the speed decrease from 85 to 31 μm s^{-1}. The 11-13-33-01 is the first transverse cross section along the 2.1-cm long translation distance where the externally imposed speed change corresponds to the 1-cm location. 69 transverse sections were carefully polished at incremental distance to obtain such microstructures. The two groves visible on the periphery of this cross-section were marked by cutting grooves along the sample length before transverse serial sectioning and helped align the transverse views with respect to each other. The colored 30 primary dendrites are the ones that were observed to disappear after the 2.1 cm location along the length.

Figure 38, shows the secondary-side arms of each of the primary dendrites in the sample 11-33-01, colored red. The green crosses correspond to those that were observed to disappear after the speed decrease.

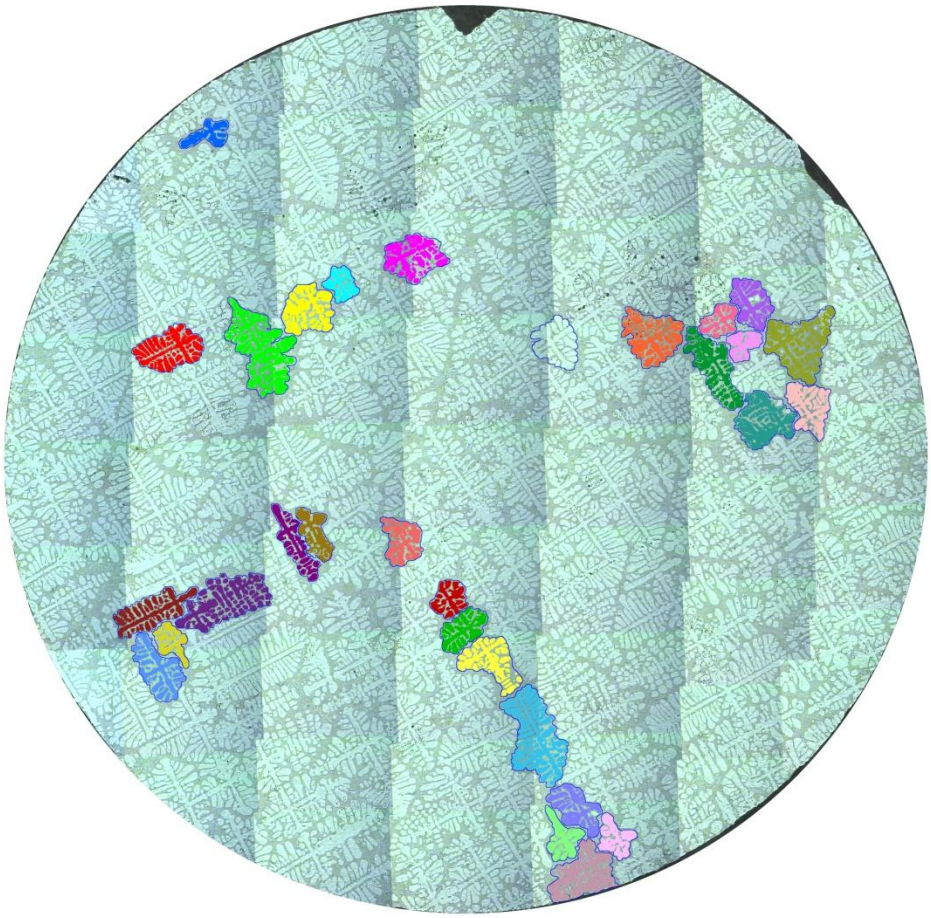

Figure 37. (11-13-33-01) transverse microstructure of an Al-7 wt% Si alloy, directionally solidified at 40 K cm^{-1}, colored primary dendrite trees are the ones that disappeared during the transient after a speed decrease from 85 to 31 μm s^{-1}.

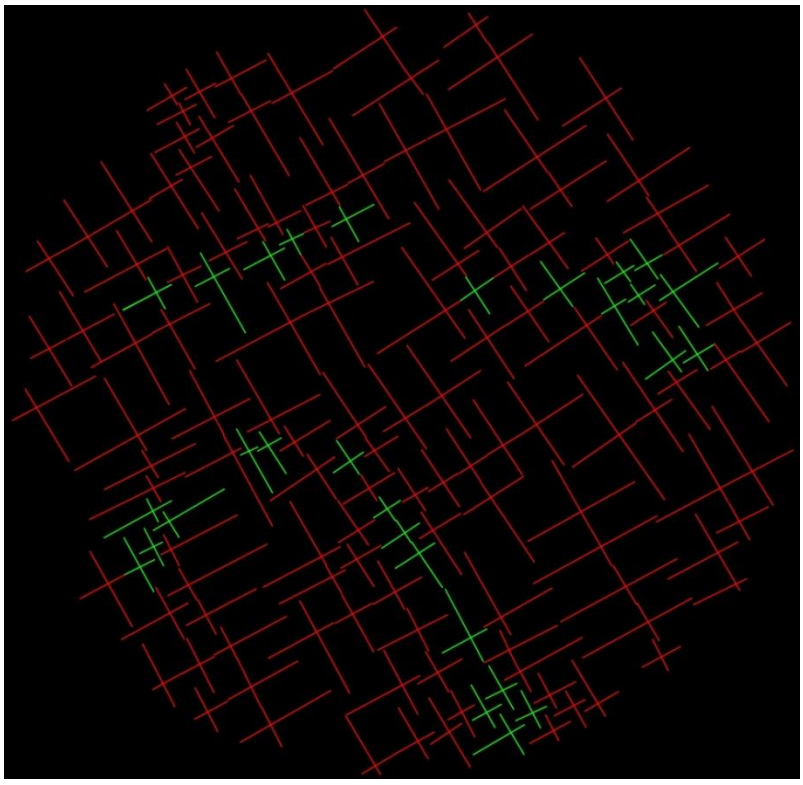

Figure 38. Distribution of side-branches (secondary dendrites) corresponding to the primary dendrites in Figure 28. Green crosses are for the disappeared primary dendrites and the red crosses are for the primary dendrites that survived 1.1 cm after the speed change.

3.8.1. Primary spacing (NNS-1, NNS-4, NNS-6)

Figure 39 presents the frequency distribution of spacing for survived and disappeared primary dendrites. The NNS-1, NNS-4, and NNS-6 represent the mean of the nearest neighbor spacing for each dendrite, mean of nearest four neighbors for each dendrite, and mean of six nearest neighbors for each dendrite respectively. These figures indicate that primary dendrites which are farther spaced are more likely to survive as compared with those are located closer to each other. The predictive abilities of NNS-1, NNS-4 or NNS-6 in terms of which dendrites are likely to dissolve off appear to be similar.

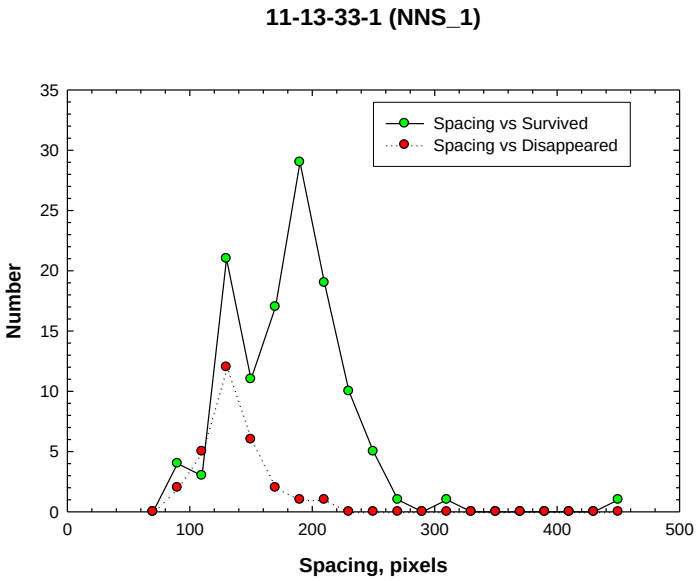
11-13-33-1 (NNS_1)
Spacing vs Survived
Spacing vs Disappeared
Number
Spacing, pixels
0
5
10
15
20
25
30
35
0
100
200
300
400
500

(a)

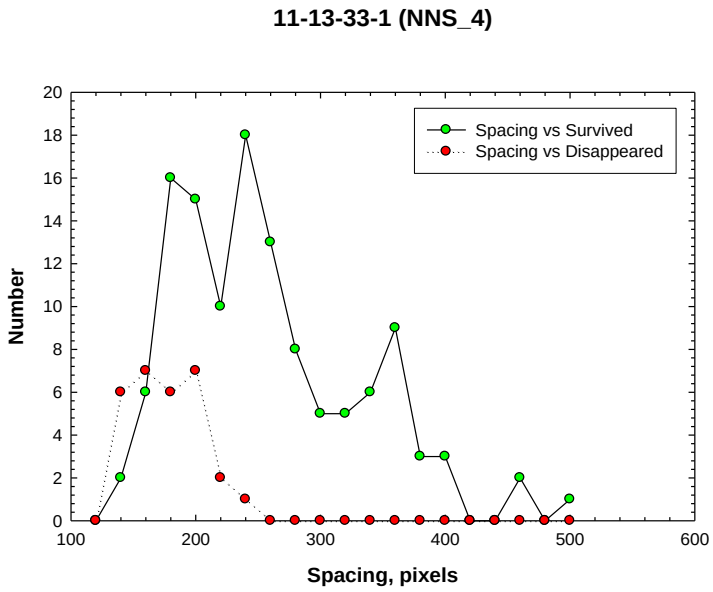
11-13-33-1 (NNS_4)
Spacing vs Survived
Spacing vs Disappeared
Number
Spacing, pixels
0
2
4
6
8
10
12
14
16
18
20
100
200
300
400
500
600

(b)

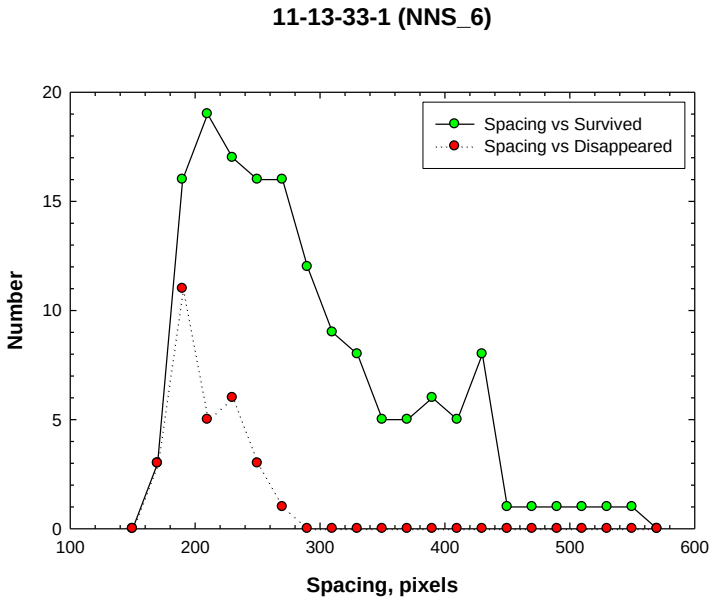

(c)

Figure 39. Frequency distribution of nearest neighbor spacing for disappeared and survived primary dendrites (Al-7 wt% Si, 40 K cm^{-1}, step decrease in growth speed from 85 to 31 μm s^{-1}).

(a)Mean of nearest neighbor spacing (NNS-1). (b)Mean of four nearest neighbor spacing (NNS-4). (c)Mean of six nearest neighbor spacing (NNS-6).

3.8.2. Side-branch length and orientation

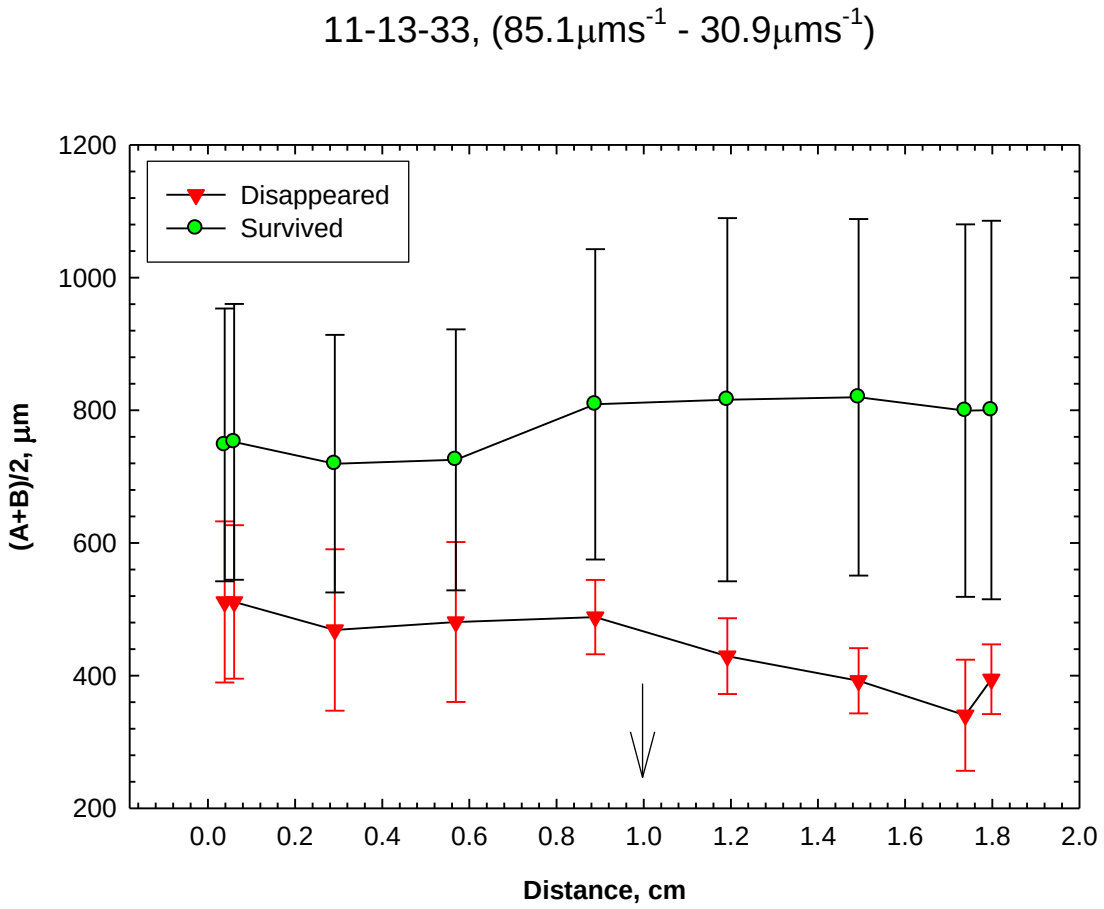

Figure 40. Comparison of mean side branch length for disappeared and survived primary dendrites (Al-7 wt% Si, 40 K cm^{-1}, step decrease in growth speed from 85 to 31 μm s^{-1}).

Figure 40 plots the mean side branch length of the primary dendrites which survived (green symbols) and those that disappeared (red symbols) as a function of distance during the transient for a step decrease in growth speed from 85 to 31 μm s^{-1}. Please note that the distance corresponding to 1-cm location corresponds to the externally imposed speed change step. The skinnier primary dendrites having smaller side-branch lengths are destined to be dissolved during the growth speed decrease transient, and those with larger side branches are likely to survive and grow. It is interesting to note that average side-branch length of the surviving trees increases whereas that of the disappearing trees

becomes smaller after the speed change. Apparently the primary dendrites with larger side arms begin to lead whereas those with smaller arms start lagging and slowly disappear from the array.

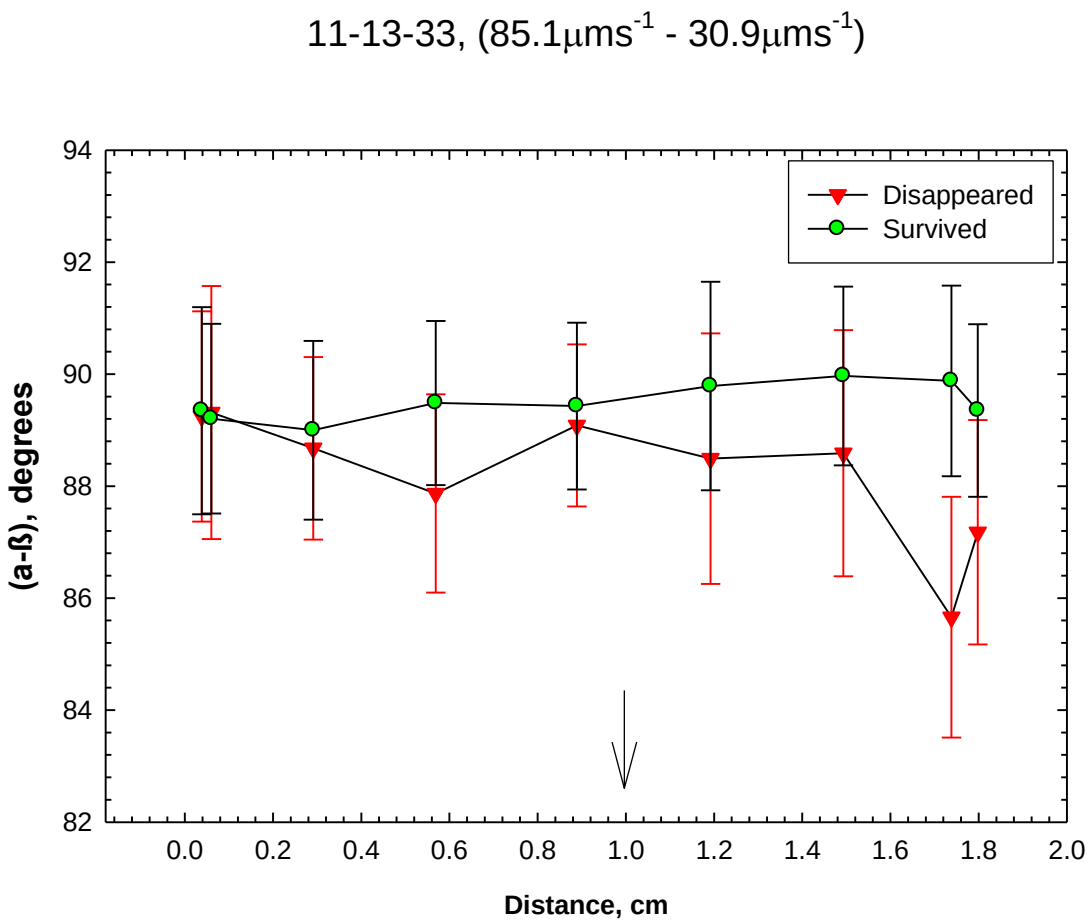

Figure 41. Comparison of side branch orientation for disappeared and survived primary dendrites (Al-7 wt% Si, 40 K cm^{-1}, step decrease in growth speed from 85 to 31 μm s^{-1}).

Figure 41 plots the difference between the two angles (α and β) for the primary dendrites which disappeared after the speed decrease (red symbols) and for those that survived (green symbols) as a function of distance. The 1-cm mark corresponds to the externally imposed step change in growth speed from 85 to 31 μm s^{-1}. Since all these transverse sections were carefully aligned with respect to each other by the help of grooves along

the sample length the angles plotted in this figure denote the true variation for these dendrites along the translation distance. This figure indicates that those primary dendrites which are not as well aligned along the growth direction, as a result their two side-arm angles don't appear exactly 90^o with respect to each other (i.e. α-$\beta < 90^o$) are more likely to dissolve-off. The primary dendrites which are disappearing along the DS length display more and more skewed (not perpendicular) side-branches.

3.9. Spurious Grain Formation

Figure 42 shows the influence of pore formation on the nucleation of spurious "misoriented" grains during steady-state arrayed growth of primary dendrites. The cross sections 11-13-33-6 through 7, 10, 13, 14, 15, 16, and 17) correspond to the same region of the sample along its directionally solidified length and cover a distance of about 3.2 mm. The Al-7% Si sample was grown at 40 K cm^{-1} and a translation rate of 85 μm s^{-1}. Pores were observed to form in otherwise well aligned primary dendrite region of this sample in cross-section 11-13-33-6. Over a relatively short distance of about 110 μm these pores first caused fragmentation of tertiary side-branches (Figure 11-13-33-10). Some fragments which may be from secondary branches are also observed. The broken off dendrite fragments apparently then became the nucleants for the completely misoriented large dendrite fragments seen Figure 11-13-33-17. These large dendrite fragments, if not remelted, during subsequent directional solidification, are potential source of "spurious' grains which are extremely detrimental to the high temperature creep properties of directionally solidified nickel based superalloy single crystal turbine blade components.

11-13-33-6

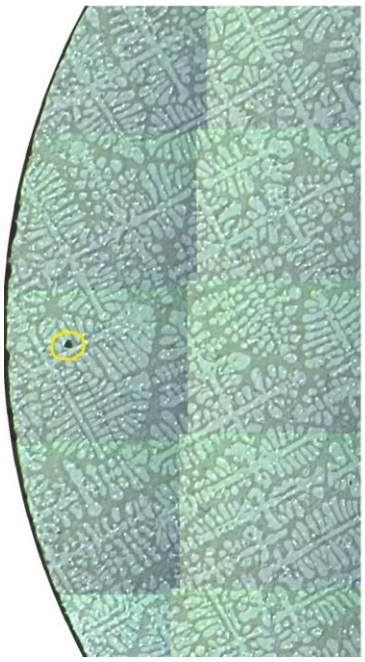

11-13-33-7

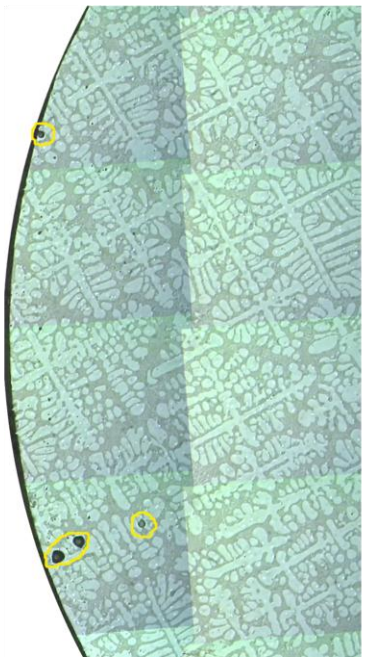

11-13-33-10

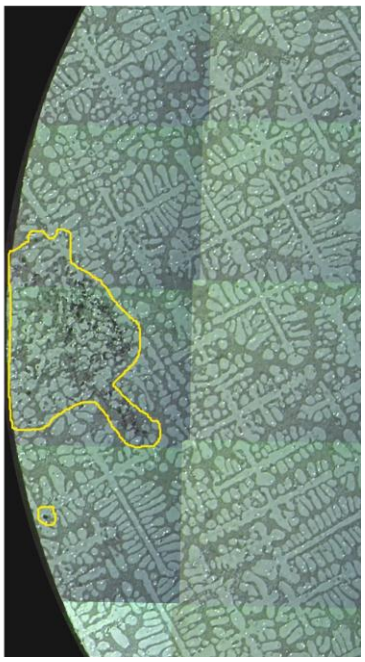

11-13-33-13

11-13-33-14

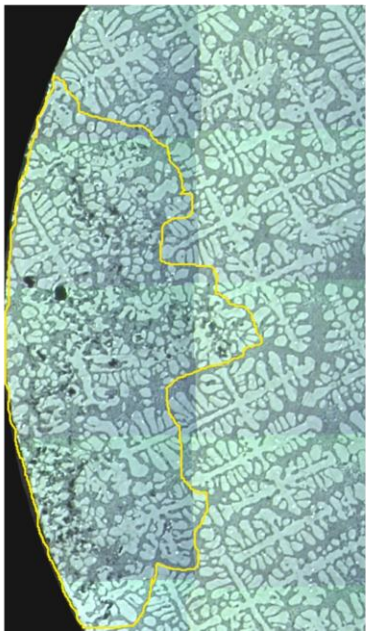

11-13-33-15

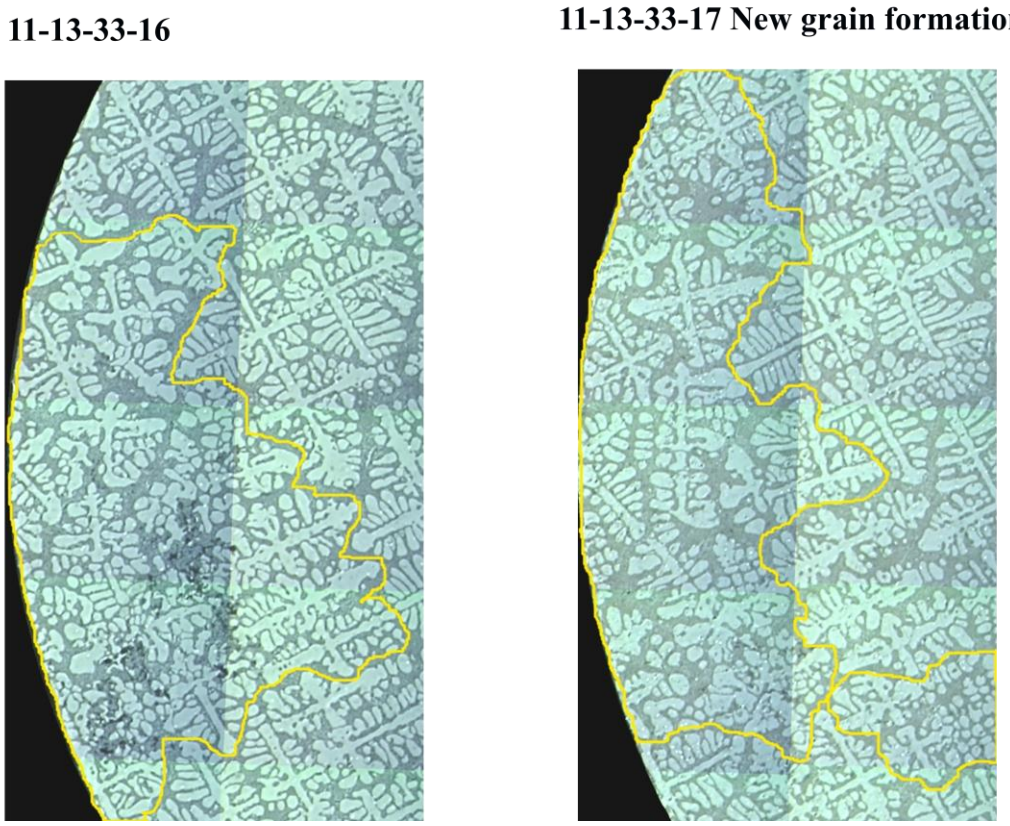

Figure 42. Influence of pore formation on the dendrite distribution and morphology (11-13-33-6, -7, -10,-13, -14, -15, -16, -17), Al-7% Si, G= 40 K cm^{-1}. The regions of interest around the pores are indicated by the yellow marking on these sections. The sections 6 through 17 cover a distance of about 3.2 mm.

CHAPTER IV

CONCLUSION

In this study, a quantitative evaluation of mushy zone morphology parameters, nearest neighbor spacing, trunk diameter, side branch length and side branch orientation of primary dendrites have been characterized in Al -7 wt % Si alloy directionally solidified at 40 K cm^{-1}along the [100] direction in order to investigate the influence of step increase and step decrease in growth speed. The following conclusions can be drawn from this evaluation.

Growth speed influences both the trunk diameter and the primary dendrite spacing in a similar manner. They both decrease with increasing growth speed. However, at any growth speed the relative scatter in the primary spacing is much larger than that in the trunk diameter. This suggests that the trunk diameter may be a better metric to quantify differences introduced by small changes in any processing parameters such as those introduced by natural convection or its absence. Since for a typical dendrite array growing in a positive thermal gradient the trunk diameters are pretty-much established

over a short distance behind the tip, the observation that the trunk diameter and theoretically predicted Hunt- Lu dendrite tip radii [12] both show a decreasing trend with increasing growth speed is to be expected. However, the ratio of trunk diameter to the theoretically predicted tip radius increases with increasing growth speed. Currently there is no theoretical analysis available to predict the primary dendrite trunk diameter during directional solidification. The slower growth speed allows for a longer time for trunk diameter coarsening to occur during solidification through the mushy zone (coarsening time = (alloy freezing range/ thermal gradient)/ growth speed). Therefore, intuitively one would expect the trunk diameter to tip radius ratio to decrease with the increasing growth speed.

The noise (standard deviation/mean) in nearest neighbor spacing distribution and the trunk diameter distribution during the transient caused by a step increase or step decrease in growth speed is larger than that observed during steady-state growth at a constant speed. A similar behavior is also observed for the dendrite trunk diameter. The relative scatter in the trunk diameter is significantly smaller than that in the nearest neighbor spacing not only during the steady-state growth but also during the transient introduced by the growth speed increase or step decrease.

The additional translation distance required for achieving a constant distribution of trunk diameter after a step increase in growth speed or a step decrease in growth speed is significantly shorter than that required for the nearest-neighbor distance distribution for the primary dendrites. For example, after a step increase in growth speed, primary trunk diameter decreased from its value of 175 μm at 4 μm s^{-1}(Figure 20) to about 68 μm for the higher speed of 85 μm s^{-1} over a distance of about 2-mm, which is considerable

smaller than the 4-cm of additional growth required for the nearest neighbor spacing to reach the new steady state [10].

A careful serial sectioning and statistical analysis of the resulting transverse array morphology after the step decrease in growth speed (from 85 to 31 μm s^{-1}) over a distance of about 2-cm showed that:

(a) After the growth speed decrease those primary dendrites with larger spacing are more likely to survive as compared with those that are located closer to each other. However, the predictive abilities of the nearest-neighbor distance (NNS-1), mean of four nearest neighbor distances (NNS-4) or mean of six nearest neighbor distances (NNS-6) in terms of which dendrites are likely to dissolve are similar.

(b) The skinnier primary dendrites having smaller side-branch lengths are destined to be dissolved during the growth speed decrease transient, and those with larger side branches are likely to survive and grow. After a speed decrease the primary dendrites with larger side arms, apparently, begin to lead whereas those with smaller arms begin to lag and slowly disappear from the array. Thus the average side-branch length of the surviving trees increases and those of the disappearing trees decreases after the speed decrease.

(c) The Primary dendrites which are not as well aligned along the growth direction, and as a result their two side-arms don't appear exactly 90^o with respect to each other (i.e. α-β< 88.8) are more likely to dissolve-off than those primary dendrites which grow exactly along [100].

Pore formation during directional solidification causes breakage of tertiary arms. Further growth of these dendrite fragments results in nucleation of mis-oriented dendrite grains. If these mis-oriented dendrites survive during further directional solidification then they may be an important cause of spurious grain formation during steady state arrayed growth of alloys. Such spurious grains are extremely detrimental to the high temperature creep properties of the directionally solidified nickel based super alloy single crystal turbine blade components in aircraft engines.

CHAPTER V

RECOMMENDATION FOR THE FUTURE RESEARCH

1) Low-gravity directional solidification experiments under similar alloy processing conditions are required to quantitatively evaluate the influence of convection. Such experiments will also elucidate the growth speed dependence of primary trunk diameter, side branch length and side branch orientation in Al-7 wt% Si alloy in the absence of convection. It could be predicted that the morphological defects on the samples grown on earth caused by natural convection will be absent in the samples grown in low-gravity ambience.

2) A systematic study needs to be conducted to investigate the nucleation of "spurious misoriented" grains from "porosity" during directional solidification, whether during step-change in growth speed or during steady-state directional solidification, since this knowledge is essential to the manufacturers of (nickel based) super alloy single crystal turbine blade components used in aircraft engines and which will also improve their high temperature creep properties.

3) Primary dendrite elimination after a step decrease in growth speed during directional solidification of alloys under a range of processing conditions requires more

quantitative micro-structural evaluation to discover the exact mechanism for their elimination.

REFERENCES

1. Flemings M. C, *Solidification processing*; McGraw-Hill: New York, 1974, pp 22.

2. Flemings M. C, Solidification Processing, *Metall Trans* **1974**, 5, pp 2121-2134.

3. Ojha, S. N.; Ding, G.; Lu, Y.; Reye, J.; Tewari, S. N. Macrosegregation Caused by Thermosolutal Convection during Directional Solidification of Pb-Sb Alloys. *Metall Mater Trans A* **1999,** 30A, pp 2167- 2171.

4. Grugel, R.N.; Brush, L.N. Observations of Macrosegregation in Directionally Solidified Dendritic alloys. *Jom-J Min Met Mat S* **1997**, 49, pp 26-30.

5. Tin, S.; Pollock, T. M. Predicting freckle formation in single crystal Ni-base superalloys. *J Mater Sci* **2004**, 39, pp 7199-7205.

6. Stanford, N.; Djakovic, A.; Shollock, B. A.; Mclean, M.; Souza, N. D.; Jennnings, P. A. Seeding of single crystal superalloys-role of seed melt-back on casting defects. *Scripta Mater***2004**, 50, pp 159-163.

7. *Metals Handbook*; *American Society for Metals*: Ohio, 1961, pp 52-53.

8. *Metals Handbook*; *American Society for Metals*: Ohio, 1973, pp 263.

9. Kurz, W.; Fisher,D.J. Fundamentals of Solidification, *Trans Tech Publications***1986**, pp 241.

10. Ravi, S. R. Directional Solidification of Al-7 wt% Si Alloy. M.S. dissertation, Cleveland State University, Cleveland, OH, 2010.

11. Grugel, N. Evaluation of Primary Dendrite Trunk Diameters in Directionally Solidified Al- Si alloys, *Mater Charact* **1992**, 28, pp 213-219.

12. Hunt, J. D.; Lu, S. Z. Numerical Modeling of Cellular/Dendrite Array Growth: Spacing and Structure Predictions, *Metall Mater Trans A***1996**,27, pp 611-623.